THESIS FOR THE DEGREE OF MASTER OF SCIENCE

DISPLOM WORK 04/17

Formulation, Implementation and Testing of $k - \omega - \overline{v^2} - f$ Model in an Asymmetric Plane Diffuser

by

OBAI YOUNIS TAHA

Department of Thermo and Fluid Dynamics
CHALMERS UNIVERSITY OF TECHNOLOGY
Göteborg, Sweden, 2004

Formulation, Implementation and Testing of $k-\omega-\overline{v^2}-f$ Model in an Asymmetric Plane Diffuser

by

Obai Younis Taha

younis@mtek.chalmers.se
Department of Thermo and Fluid Dynamics
Chalmers University of Technology
SE-412 96 Göteborg
Sweden

Abstract

Most of the low Reynolds turbulence models contain an ad hoc viscous damping function in the eddy viscosity expression, which corrects the improper asymptotic behavior of the eddy viscosity formulation when approaching a solid wall. The damping function is often non-linear and causes numerical stiffness. In the $\overline{v^2}-f$ model – originally suggested by Durbin – the use of damping function is avoided by choosing $\overline{v^2}$ (the turbulence stress normal to the wall) to be the velocity scale rather than k.

All the recent $\overline{v^2}-f$ models are based on $k-\varepsilon$ model. Although these models showed a good performance in many engineering applications, they still suffer from two drawbacks. The first drawback is that they can be numerically unstable for grids with well resolved wall region. The second is the uncertainty in specifying the wall boundary condition of ε. In the present thesis, a new $\overline{v^2}-f$ model based on the standard $k-\omega$ model and referred to as $k-\omega-\overline{v^2}-f$ model is formulated which has numerically appealing boundary condition for ω. A new set of model constants are determined by tuning the result to match the DNS data of fully developed channel flow. The $k-\omega-\overline{v^2}-f$ model showed quantitatively good results in a fully developed channel flow $(Re=6000)$.

In order to validate the $k-\omega-\overline{v^2}-f$ model, numerical simulations of a well documented separated flow in asymmetric plane diffuser have been preformed. The results obtained are discussed and a qualitative comparison with the experimental data is made. The results are shown to be in a good agreement with the experimental data.

Acknowledgments

I would like to acknowledge my supervisor Prof. Lars Davidson for his guidance, support and for his valuable comments. I specially thank him for his wonderful perpetual readiness to help others and for being always smiling.

I would also like to thank the PhD student Andreas Sveningsson for shearing me not only his office but also his knowledge, and for helping me in virtually every thing.

I am also grateful to Prof. William K. George for his great lectures on Turbulence, encouragement and endless support not just in academics but in different aspects of life.

I would also like to express my sincere gratitude to Associate Prof. Dr. Gunnar Johansson.

My thanks extend to the Sudanese community and CIF members in Göteborg for providing me with the social environment, that I've never felt away from home.

Lastly but first in mind, I would like to express my gratitude to my parents, my brother, my sisters and in particular my wife for their unconditional love and support.

Contents

Chapter 1

Introduction

1.1 Turbulence

It is well known from experiments on fluids system that at values below the so-called critical Reynolds number the flow is smooth and adjacent layers of fluid slide past each other in orderly fashion. If the applied boundary conditions do not change with time the flow is steady. This kind of flow regime called laminar flow.

At values of the Reynolds number above the critical Reynolds number the flow behavior is totally different, and a complicated series of events take place which leads to a radical change in the flow character. In the final state the flow behavior is random and chaotic. The motion becomes intrinsically unsteady even with constant imposed boundary conditions. And the flow properties start to vary in random way. Such kind of regime is called turbulent.

It is not an easy task to find a proper definition of turbulence. However, in 1937 Taylor and von Karman proposed the following definition: "Turbulence is an irregular motion which is general makes it is appearance in fluids, gaseous or liquid, when they flow past solid or surface or even when neighboring streams of the same fluid flow past over one another" [4].

1.2 Why do we need Turbulence Modeling

Although the well known Navier-Stokes (N-S) equations describe the details of turbulent motions, it is too costly and often time consuming for engineers to solve such complex and detailed equations (DNS). Instead, ensemble-averaged N-S equations are often sufficient and practical to describe the turbulent motion in engineering problems. Unfortunately the averaging process generates additional unknown quanti-

ties and the set of equations is unclosed due to the appearance of these new unknowns. Hence modeling approach is needed to obtain closed set of equations. In the present work the eddy viscosity concept is used. This will be discussed further in details in this chapter.

1.3 Motivation and Objective

Although most of the two equation eddy viscosity models can be solved all the way down to the wall, it does not give a quantitatively good behavior in the near wall region . This is mainly because the two-equations model have not been designed to account for the wall echo effects. To take into account the influence of the wall, usually arbitrary damping functions are introduced.

In order to simulate turbulent flows, taking into account anisotropy non-local effects, the $\overline{v^2}-f$ model was introduced by Durbin [23]. In this model the system of equations of the Reynolds stress tensor is replaced by a transport equation for the velocity scalar $\overline{v^2}$ and an elliptic equation is introduced for a function f. The model represents the transport suppression made by the wall in the normal direction. By representing this effects and choosing $\overline{v^2}^{\frac{1}{2}}$ as a velocity scale the damping of the eddy viscosity is no longer needed. Figure 1.1 clarifies the role of the damping function and explains the main motivation of working with the $\overline{v^2}-f$ model. The figure shows the eddy viscosity computed from the DNS data [25] using three different formulas. The DNS eddy viscosity was computes as $\nu_t = -\overline{uv}/\frac{\partial U}{\partial y}$, the $k-\varepsilon$ eddy viscosity was computed as $\nu_t = C_\mu k^2/\varepsilon$ and the $\overline{v^2}-f$ was computed as $\nu_t = C_\mu \overline{v^2} k/\varepsilon$. It is clear as pointed by Durbin [23] that the $k-\varepsilon$ model fails to predict the true eddy viscosity close to the wall because k^2/ε has the wrong profile of as a function of y^+ while the $\overline{v^2}-f$ model almost reproduced the true eddy viscosity near the wall. Thus if we can model $\overline{v^2}$, the need for a damping function can be avoided [23]. All the $\overline{v^2}-f$ models of today are based on $k-\varepsilon$ model. The $\overline{v^2}-f$ model may be considered as a modification of the $k-\varepsilon$ model to account of near wall anisotropy effects. Although the model had been used in several CFD problems and showed encouraging results e.g. in aerospace configurations [9] and flows with adverse pressure gradient [24], it has two major drawbacks. The first drawback is associated with its boundary conditions for ε which reads

$$\varepsilon = \nu \frac{2k}{y^2} \quad \text{as} \quad y \to 0.$$

During the iterative process the boundary value of ε keeps on changing

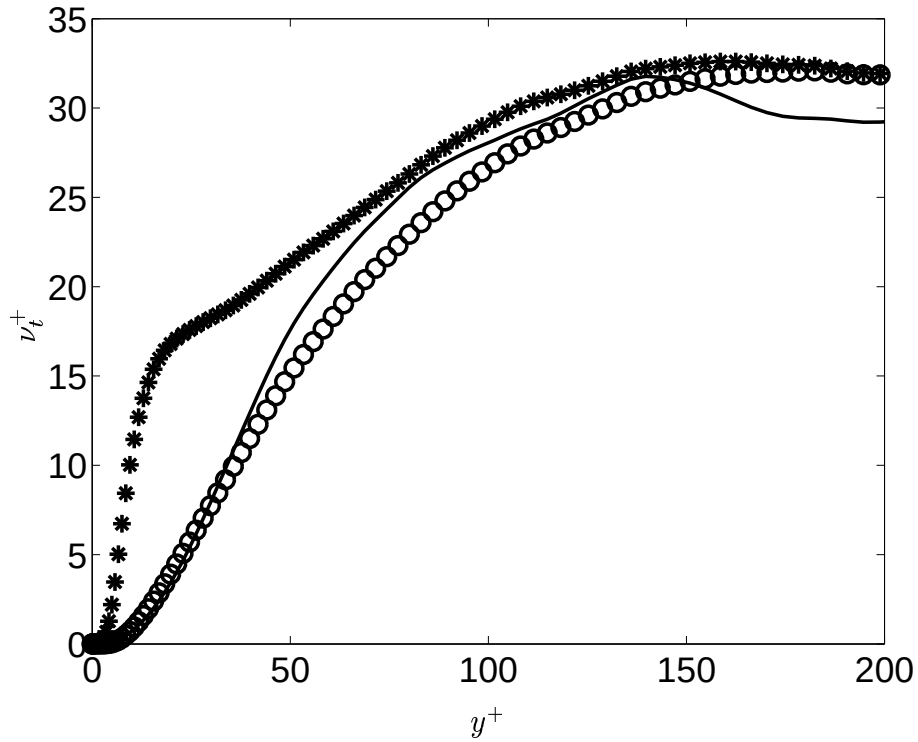

Figure 1.1: Normalized turbulent eddy viscosity for different ν_t closures computed from DNS data. Solid line: DNS; $*$: $k-\varepsilon$; $\circ$: $\overline{v^2}-f$.

due to the appearance of k which is also changing. Meanwhile the f equation is highly diffusive in nature and very sensitive to the changes in ε. The coupling between ε and f near the wall causes numerical difficulties. The second drawback is that the model is very sensitive to the quality of of the mesh, especially in the near-wall region [1].

These kinds of problems lead to the idea of formulating the $k-\omega-\overline{v^2}-f$ model, the main encouraging feature with this model is the boundary condition of ω which reads

$$\omega = \frac{6\nu}{\beta y^2} \quad \text{as} \quad y \to 0.$$

ν is fluid property and always constant, and for given mesh y is also constant and hence the boundary condition of ω is constant during the iterative process.

In order to validate the model a test case with experimental data is needed. The main objective of this work is to formulate the $k-\omega-\overline{v^2}-f$ model, test its performance on separated flow in asymmetric plane diffuser and compare the results to two sets of experimental data by Obi. et. al [22] and Buice & Eaton [2].

Chapter 2

Governing equations

The fluid motion is governed by two equations, the continuity equation and the the momentum equation which read

$$\tilde{\rho}\left[\frac{\partial \tilde{u}_i}{\partial t} + \tilde{u}_j \frac{\partial \tilde{u}_i}{\partial x_j}\right] = -\frac{\partial \tilde{p}}{\partial x_i} + \frac{\partial \tilde{T}_{ij}^{(v)}}{\partial x_j} \tag{2.1}$$

$$\left[\frac{\partial \tilde{\rho}}{\partial t} + \tilde{u}_j \frac{\partial \tilde{\rho}}{\partial x_j}\right] + \tilde{\rho}\frac{\partial \tilde{u}_j}{\partial x_j} = 0 \tag{2.2}$$

Tilde denotes that the instantaneous value of the variable.

If he fluid is Newtonian, the viscous stress can be related to the fluid motion via the molecular viscosity.

$$\tilde{T}_{ij}^{(v)} = 2\mu\left(\tilde{s}_{ij} - \frac{1}{3}\tilde{s}_{kk}\delta_{ij}\right) \tag{2.3}$$

The rate of strain tensor $\tilde{s}_{ij}$ is defined by

$$\tilde{s}_{ij} = \frac{1}{2}\left(\frac{\partial \tilde{u}_i}{\partial x_j} + \frac{\partial \tilde{u}_j}{\partial x_i}\right) \tag{2.4}$$

Considering incompressible fluids (the density is independent of the pressure) all derivatives of $\tilde{\rho}$ is zero and the governing equations are simplified to

$$\left[\frac{\partial \tilde{u}_i}{\partial t} + \tilde{u}_j \frac{\partial \tilde{u}_i}{\partial x_j}\right] = -\frac{1}{\rho}\frac{\partial \tilde{p}}{\partial x_i} + \nu\frac{\partial^2 \tilde{u}_i}{\partial x_j^2} \tag{2.5}$$

$$\frac{\partial \tilde{u}_j}{\partial x_j} = 0 \tag{2.6}$$

2.1 Reynolds Averaging

When measuring flow quantities we are usually interested in the mean values rather Reynolds than the time histories. Therefore we introduce statistical tools to study turbulence and to decompose the instantaneous variables into a mean value and fluctuating value

$$\begin{aligned} \tilde{u}_i &= U_i + u_i \\ \tilde{p}_i &= P + p \end{aligned} \tag{2.7}$$

This averaging concept was introduced by Reynolds and is referred to as Reynolds decomposition.
Inserting equation (2.7) into equation (2.5) and equation (2.6) and time averaging we obtain Reynolds Averaged Navier-Stokes equation (RANS)

$$\left[\frac{\partial U_i}{\partial t} + U_i \frac{\partial U_j}{\partial x_j}\right] = -\frac{1}{\rho}\frac{\partial P}{\partial x_i} + \nu \frac{\partial^2 U_i}{\partial x_i^2} - \frac{\partial}{\partial x_j}\overline{u_i u_j} \tag{2.8}$$

$$\frac{\partial U_j}{\partial x_j} = 0 \tag{2.9}$$

A new term $\overline{u_i u_j}$ appears on the right hand side of equation (2.8) which is called the Reynolds stress tensor. It represents all effects of turbulent fluid motion on the averaged flow field. The averaging process generated six unknowns terms (Reynolds stress tensor). Now the number of unknowns (three velocities, pressure and six Reynolds stresses) is greater than the number of equations (three components of Navier-Stokes equation and the continuity equation). This is called the closure problem. In order to obtain a closed set of equations the Reynolds stresses must be related to other known variables. In the present work the eddy viscosity concept is used to model the Reynolds stresses.

2.2 Eddy viscosity

In a turbulent flow the generation of Reynolds stresses is proportional to the mean rate of strain. If we assume that the turbulence responds rather quickly to changes in the mean flow we would expect the Reynolds themselves to be related to the mean rate of strain.

In the eddy viscosity turbulence models the Reynolds stresses are linked to the velocity gradient via the turbulent viscosity. This relation is called Boussinesq assumption, where the Reynolds stress tensor from the time averaged Navier-Stokes equation is replaced by the turbulent viscosity multiplied by velocity gradient

$$\overline{u_i u_j} = -2\nu_t S_{ij} + \frac{2}{3} k \delta_{ij} \tag{2.10}$$

The eddy viscosity is treated as a scalar quantity and given by

$$\nu_t = C_\mu v^2 T \tag{2.11}$$

where v and T are a turbulent velocity scale and a time scale, respectively. C_μ is supposed to be a universal constant. Choosing a proper velocity scale and time scale depends on which turbulence model we are using.

Chapter 3

Numerical methods

3.1 CALC-BFC Solver

The in-house incompressible finite volume code CALC-BFC (Boundary Fitted Coordinates) [18] is employed to carry out the computations in this work. The code utilizes the collocated variable arrangement. The governing equations are written in a non-orthogonal coordinates system. The finite volume method is used to transform the partial differential equations to algebraic relations. The TDMA (Tri-Diagonal Matrix Solver) is employed to solve the obtained algebraic relation. To approximate the fluxes three differencing schemes are available: the hybrid scheme, the van Leer scheme and the Quick scheme. The linkage of the velocities and pressure is handled by SIMPLEC. Rhie & Chow interpolation method is used to overcome the pressure field oscillations.

3.2 The finite volume method

Let Φ be any dependent scalar variable. The transport equation of Φ reads

$$\frac{\partial}{\partial t}(\rho\Phi) + \frac{\partial}{\partial x_i}\left(\rho u_i \Phi - \Gamma_\Phi \frac{\partial \Phi}{\partial x_i}\right) = S_\Phi \tag{3.1}$$

Defining the convective and diffusive flux as

$$I_i = \rho u_i \Phi - \Gamma_\Phi \frac{\partial \Phi}{\partial x_i} \tag{3.2}$$

For steady state the term involving time derivative vanishes. Using equation (3.2), equation (3.1) can be written as

$$\frac{\partial I_i}{\partial x_i} = S_\Phi \tag{3.3}$$

Integration of equation (3.3) over a control volume in the physical space, using Gauss' theorem

$$\int_V \frac{\partial I_i}{\partial x_i} dV = \int_A I_i A_i$$

yields

$$\int_A I_i dA_i = \int_V S dV \tag{3.4}$$

The integral above yields the discretized equation.

$$\sum_{faces} (I_i A_i)_{face} \quad = S\delta V \tag{3.5}$$

Equation (3.5) is rearranged using the differencing scheme for I_i, to the standard form.

$$a_p \Phi_p = \sum_{NB} a_{NB} \Phi_{NB} + S\delta V \tag{3.6}$$

Equation (3.6) is solved with the iterative methods to obtain the approximate solution of the transport equation (3.1).

3.3 The differencing schemes

The differencing scheme is introduced to calculate the convective and diffusive flux in-order to solve the discretized equation. In the collocated grid arrangements all the variables are stored at the nodes, while the fluxes are calculated at the faces of the control volumes. Interpolation function is needed to obtain the variables on the faces. This interpolation function is known as differencing scheme. In the following section the differencing schemes used in CALC-BFC are described. Since we are working with the finite volume method all the differencing schemes are conservative.

3.3.1 The central differencing scheme

The central differencing scheme approximates the face value by using linear interpolation.

$$\Phi_e = (1 - f_e)\Phi_P + f_e \phi_E$$

where

$$f_e = \frac{\delta x_{Pe}}{\delta x_{PE}}$$

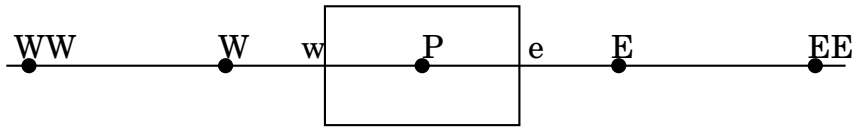

Figure 3.1: Grid nomenclature. Small letters denote the faces of the control volumes and the capital letters denote the nodes.

The central differencing scheme has two major drawbacks. The first one is that it is unbounded (possibility of negative coefficient) which can lead to oscillations and numerical problems. The second one is that it is not transportive which means it is unable to identify the flow direction.

3.3.2 The upwind differencing scheme

In this scheme the face values are set equal to the upwind nodes as:

$$\Phi_e = \Phi_P \text{ if } U_e \geq 0$$

$$\Phi_e = \Phi_E \text{ if } U_e \leq 0$$

The upwind differencing scheme is bounded and transportive. The only drawback is that it is first order accurate.

3.3.3 The hybrid differencing scheme

The hybrid differencing scheme of Spalding is a blend of central and upwind differencing scheme. The central differencing scheme is used when the Peclet number is small $Pe \leq 2$, and the upwind differencing scheme is used for large Peclet numbers $Pe \geq 2$.

$$\Phi_e = \Phi_P \text{ if } U_e \geq 2 \text{ and } \mid Pe_e \mid \geq 0$$

$$\Phi_e = \Phi_E \text{ if } U_e \leq 2 \text{ and } \mid Pe_e \mid \geq 0$$

$$\Phi_e = f_x \Phi_E + (1 - f_x)\phi_P \text{ for } \mid Pe_e \mid \leq 2$$

The Peclet number is defined as the ratio of the convective flux to the diffusive flux.

$$Pe = \rho u / \left(\frac{\Gamma}{\delta x} \right)$$

The major drawback of hybrid scheme is that the convection is always dominating so that the scheme becomes first order accurate.

3.3.4 The van Leer scheme

This scheme of van Leer is of second order accuracy accuracy except at local minima and maxima where the accuracy is of first order. One advantage of this scheme is that it is bounded.

For the east face it can be written as:

$$U_e \geq 0 \rightarrow \begin{cases} \Phi_e = \Phi_P & \text{if } |\Phi_E - 2\Phi_P + \phi_W| \geq |\Phi_E - \Phi_W| \\ \Phi_e = \Phi_P + \frac{(\Phi_E - \Phi_P)(\Phi_P - \Phi_W)}{\Phi_E - \Phi W} & \text{otherwise} \end{cases}$$

$$U_e \leq 0 \rightarrow \begin{cases} \Phi_e = \Phi_E & \text{if } |\Phi_P - 2\Phi_E + \phi_{EE}| \geq |\Phi_P - \Phi_{EE}| \\ \Phi_e = \Phi_E + \frac{(\Phi_P - \Phi_E)(\Phi_E - \Phi_{EE})}{\Phi_P - \Phi EE} & \text{otherwise} \end{cases}$$

3.4 SIMPLEC algorithm

The solution of the discretized equations depends on the pressure distribution, which must be solved together with the velocity fields. In incompressible flow there is no equation for the pressure and some kind of velocity coupling is needed. In CALC-BFC the pressure velocity coupling is introduced by the SIMPLEC method (Semi-Implicit Method for Pressure-Linked Equations, Consistent) [27].

The method has its origin in staggered grid methodology and is adapted to collocated grid methodology through the use of Rhie & Chow interpolation. For simplicity the derivation of SIMPLEC will be carried out only for the staggered control volume e (face e in the collocated grid arrangement).

Defining the pressure and velocity corrections, p' and u_i', as the difference between the pressure and the velocity field, p and u_i, at the current iteration and the pressure and velocity field at the previous iteration, p^* and u_i^*.

$$p = p^* + p', u_i = u_i^* + u_i' \tag{3.7}$$

The discretized momentum equation for the velocity of the previous iteration reads.

$$a_e u_{ie}^* = \sum a_{nb} u_{inb}^* + (p_P^* - p_E^*) A_{ie} + b_e \tag{3.8}$$

where b_e is the momentum source term.
The discretized momentum equation for the velocity of the new iteration reads:

$$a_e u_{ie} = \sum a_{nb} u_{inb} + (p_P - p_E) A_{ie} + b_e \tag{3.9}$$

By subtracting equation (3.8) from equation (3.9) we obtain.

$$a_e u_{ie}' = \sum a_{nb} u_{inb}' + (p_P' - p_E') A_{ie} \tag{3.10}$$

Subtracting the term $\sum a_{nb}u'_{ie}$ from both sides of equation (3.10) yields.

$$\left(a_e - \sum a_{nb}\right) u'_{ie} = \sum a_{nb}(u'_{inb} - u'_{ie}) + (p'_P - p'_E)A_{ie} \tag{3.11}$$

The omission of the term $\sum a_{nb}(u'_{inb} - u'_{ie})$ yields:

$$u'_{ie} = \frac{A_{ie}}{a_e - \sum a_{nb}} (p'_P - p'_E) \tag{3.12}$$

where $a_e = a'_e/\alpha$ and α is the velocity underrealxation factor.
By inserting equation (3.12) into equation (3.7) we obtain the final expression of the new (at the current iteration) face velocity:

$$u_{ie} = u^*_{ie} + d_e(p'_P - p'_E) \tag{3.13}$$

where

$$d_e = \frac{A_{ie}}{a_e - \sum a_{nb}}$$

Inserting the corrected velocities into the discretized continuity equation of collocated control volumes yields

$$\sum_{C.S}(\rho u_{inb}A_{inb}) = 0$$

Identifying coefficients gives a discretized equation for the pressure correction (in 1D form).

$$a_p p'_P = a_E p'_E + a_W p'_W + b_{p'\,P} \tag{3.14}$$

where

$$a_P = a_E + a_W$$

$$a_E = \rho_e \frac{A_e^2}{a_e - \sum a_{nb}}$$

$$a_W = \rho_w \frac{A_w^2}{a_w - \sum a_{nb}}$$

$$b_{p'\,P} = -\sum_{C.S}(\rho u^*_{inb}A_{inb})$$

This Poisson equation for the pressure correction is solved using a_{nb} and u^*_{inb} values from the momentum equations. The a_{nb} values are obtained from linear interpolation of a_P values and u_{inb} values are obtained by Rhie & Chow interpolation of u_{iP} values. Then the new pressure field is obtained from equation (3.7) and the velocities are corrected according to equation (3.13).

3.5 Rhie & Chow interpolation

As mentioned before, CALC-BFC utilizes a collocated grid arrangement. The Rhie & Chow interpolation is introduced to obtain the convection through the faces needed in the pressure correction equation. A brief description of this interpolation is given below.

Usually the face velocity is always obtained by linear interpolation. For the east face it reads.

$$u_{ie} = \frac{1}{2}(u_{iE} + u_{iP})$$

In the collocated grid arrangement, however, this may lead to pressure oscillations. To avoid this, the face velocities are calculated by subtracting and adding the pressure gradient.

$$u_{ie} = \frac{1}{2}(u_{iE} + u_{iP}) - \left(-\frac{\partial p}{\partial x_i}\frac{\partial V}{a_P}\right)_e + \left(-\frac{\partial p}{\partial x_i}\frac{\partial V}{a_P}\right)_e$$

The pressure terms in this expression are calculated in different ways. The first is calculated as the mean value of the pressure gradient in the P and E nodes.

$$\left(-\frac{\partial p}{\partial x_i}\frac{\partial V}{a_P}\right)_e = -\frac{1}{2}\left(\frac{p_{EE} - p_P}{\delta x_{iPEE}} + \frac{p_E - p_W}{\delta x_{iWE}}\right)\left(\frac{\delta V}{a_P}\right)_e$$

The second is calculated on the face.

$$\left(-\frac{\partial p}{\partial x_i}\frac{\partial V}{a_P}\right)_e = -\left(\frac{p_E - p_P}{\delta x_{iPE}}\right)\left(\frac{\delta V}{a_P}\right)_e$$

And for equidistant grid.

$$u_{ie} = \frac{1}{2}(u_{iE} + u_{iP}) + \frac{1}{\delta x_{iPE}}\left(\frac{\delta V}{a_P}\right)_e (p_{EE} - 3p_E + 3p_p - p_W)$$

In the case of non-equidistant grids, the first term is calculated as a weighted average and the second term is included as it is.

3.6 TDMA Solver

The discretization process applied on the governing equations of the fluid flow results in linear algebraic equations which need to be solved. Mainly there are two families of solution techniques : direct methods and indirect or iterative methods. One of the most interesting features

in the iterative methods is that only non-zero coefficient of the equations need to be stored in core memory.

The TDMA is a direct method for one dimensional cases, but at the same time it can be applied iteratively in a line-by-line fashion to solve multi dimensional problems. It is computationally inexpensive and requires a minimum amount of storage.

CALC-BFC employed the segregated TDMA as a matrix solver which is described below (for 2D case for simplicity).
The 2D discretized equation for property ϕ reads

$$a_P\phi_P = a_E\phi_E + a_W\phi_W + a_N\phi_N + a_S\phi_S + S_U \tag{3.15}$$

Equation (3.15) can be written in the form

$$a_i\phi_i = b_i\phi_{i+1} + c_i\phi_{i-1} + d_i \tag{3.16}$$

where

$$a_i = a_P, b_i = a_E, c_i = a_W$$

$$d_i = a_N\phi_N + a_S\phi_S + S_U$$

Again we can rewrite equation (3.16) as

$$\phi_i = P_i\phi_{i+1} + Q_i \tag{3.17}$$

In order to put equation (3.16) in the form of equation (3.17) we need to write equation (3.16) in a matrix form and apply elimination techniques. Equation (3.16) in matrix form reads

$$\begin{bmatrix} a_2 & -b_2 & 0 & \dots & & \\ -c_3 & a_3 & -b_3 & 0 & \dots & \\ 0 & -c_4 & a_4 & -b_4 & 0 & \dots \\ \vdots & \vdots & \vdots & \vdots & \vdots & \vdots \end{bmatrix} \begin{bmatrix} \phi_2 \\ \phi_3 \\ \phi_4 \\ \vdots \end{bmatrix} = \begin{bmatrix} d_2 + c_2\phi_1 \\ d_3 \\ d_4 \\ \vdots \end{bmatrix} \tag{3.18}$$

Divide the first row by a_2

$$\begin{bmatrix} 1 & -P_2 & 0 & \dots & & \\ -c_3 & a_3 & -b_3 & 0 & \dots & \\ 0 & -c_4 & a_4 & -b_4 & 0 & \dots \\ \vdots & \vdots & \vdots & \vdots & \vdots & \vdots \end{bmatrix} \begin{bmatrix} \phi_2 \\ \phi_3 \\ \phi_4 \\ \vdots \end{bmatrix} = \begin{bmatrix} Q_2 \\ d_3 \\ d_4 \\ \vdots \end{bmatrix} \tag{3.19}$$

where

$$P_2 = \frac{b_2}{a_2}, Q_2 = \frac{d_2 + c_2\phi_1}{a_2}$$

In order to eliminate the $c's$ multiply the first row by c_3, add it to the second row and then divide the second row by $a_3 - c_3P_2$.

$$\begin{bmatrix} 1 & -P_2 & 0 & \dots & & \\ 0 & 1 & -P_3 & 0 & \dots & \\ 0 & -c_4 & a_4 & -b_4 & 0 & \dots \\ \vdots & \vdots & \vdots & \vdots & \vdots & \vdots \end{bmatrix} \begin{bmatrix} \phi_2 \\ \phi_3 \\ \phi_4 \\ \vdots \end{bmatrix} = \begin{bmatrix} Q_2 \\ Q_3 \\ d_4 \\ \vdots \end{bmatrix} \tag{3.20}$$

where

$$P_3 = \frac{b_3}{a_3 - c_3P_2}, Q_3 = \frac{d_3 + c_3Q_2}{a_3 - c_3P_2}$$

Now equation (3.20) becomes an recursive equation for P_i and Q_i on the form

$$P_i = \frac{b_i}{a_i - c_iP_{i-1}}, Q_i = \frac{d_i + c_iQ_{i-1}}{a_i - c_iP_{i-1}}$$

Chapter 4

Turbulence models

The Reynolds averaging introduced in chapter 2 results in appearance of new unknown terms (Reynolds stresses) which need to be modeled. A turbulence model is a computational procedure to close the system of the mean flow equations. For a turbulence model to be useful in a general purpose CFD code it must have wide applicability, be accurate, simple and economical to run. According to Versteeg [13], the most common turbulence models are classified to:

- Classical models.
    1. Zero equation model.
    2. Two equation model.
    3. Reynolds stress equation model.
    4. Algebraic stress model.
- Large eddy simulation.

The computations in the present thesis have mainly been carried out using two different $\overline{v^2} - f$ models. However the standard $k - \varepsilon$ and $k - \omega$ models (under the two -equation model category) are introduced below because they form the basis for the advanced $\overline{v^2} - f$ models. And also they have been used to provide the initial solution for the $\overline{v^2} - f$ models.

4.1 Two-equation models

Researchers in turbulent flow have long felt that the length scale in turbulence models should depend on upon upstream history of the flow and not just local flow conditions (as in algebraic mixing-length model).

An obvious way to provide more complex dependence of the length scale l on he flow is to derive a transport equation for the variation of l. The equation from which the length scale is obtained is a partial differential equation and the model is then referred to as a two-equation model.

Although a transport partial differential equation can be developed for a length scale, the terms in this equation are not easily modeled, and some workers have experienced better success by solving a transport equation for a length scale related parameter rather than the length scale itself, i.e, ε and ω as in $k-\varepsilon$ and $k-\omega$ models.

4.1.1 The standard $k-\varepsilon$ model

$k-\varepsilon$ model is the most popular two-equation model. The model had been developed by many turbulence researchers such as Chou and Davidov. Jones and Launder [14] introduced the standard $k-\varepsilon$ model.

The model is based mainly on the exact transport equation of the kinetic energy k and the dissipation rate ε. The ε equation was chosen to determine the turbulent length scale l as it appears naturally in the k equation. The turbulent eddy viscosity is obtained by choosing $k^{1/2}$ to be the velocity scale and k/ε to be the time scale. The model equations read

$$U_j\frac{\partial k}{\partial x_j}=\frac{\partial}{\partial x_j}\left(\left(\nu+\frac{\nu_t}{\sigma_k}\right)\frac{\partial k}{\partial x_j}\right)+P_k-\varepsilon \tag{4.1}$$

$$U_j\frac{\partial \varepsilon}{\partial x_j}=\frac{\partial}{\partial x_j}\left(\left(\nu+\frac{\nu_t}{\sigma_\varepsilon}\right)\frac{\partial \varepsilon}{\partial x_j}\right)+\frac{C_{\varepsilon 1}P_k}{T}-\frac{C_{\varepsilon 2}\varepsilon}{T} \tag{4.2}$$

The eddy viscosity is given by

$$\nu_t=C_\mu\frac{k^2}{\varepsilon} \tag{4.3}$$

The length scale is given by

$$l=\frac{k^{\frac{3}{2}}}{\varepsilon} \tag{4.4}$$

The closure coefficients

$$C_{\epsilon 1}=1.44,\ C_{\epsilon 2}=1.92,\ C_\mu=0.09,\ \sigma_k=1.0,\ \sigma_\varepsilon=1.3$$

ε boundary condition

One could derive the wall boundary condition of ε by examining equation (4.1) in the near wall region. As $y\to 0$, all terms vanish except the viscous diffusion term and the dissipation term.

$$\nu\frac{\partial^2 k}{\partial y^2}-\varepsilon=0 \tag{4.5}$$

which directly gives

$$\varepsilon = \nu \left(\frac{\partial^2 k}{\partial y^2} \right)_{wall} \tag{4.6}$$

This type of boundary condition can be numerically unstable, since it relies on the evaluation of a second derivative at the wall [17].

An alternative wall boundary conditions for ε could be obtained by applying Taylor expansion to the fluctuating velocities.

$$\begin{aligned} u &= a_o + a_1 y + a_2 y^2 + \dots \\ v &= b_o + b_1 y + b_2 y^2 + \dots \\ w &= c_o + c_1 y + c_2 y^2 + \dots \end{aligned} \tag{4.7}$$

At the wall the fluctuating velocities $= 0$ due to the no-slip condition, which gives $a_o = b_o = c_o = 0$. Furthermore, at the wall $\partial u/\partial x = \partial w/\partial z = 0$ and the continuity gives $\partial v/\partial y = 0$. Therefore $b_1 = 0$. The behavior of Reynolds stress component at the wall is found by squaring and averaging equation (4.7)

$$\begin{aligned} \overline{u^2} &= \overline{a_1^2} y^2 + \mathcal{O}(y^3) \\ \overline{v^2} &= \overline{b_2^2} y^4 + \mathcal{O}(y^5) \\ \overline{w^2} &= \overline{c_1^2} y^2 + \mathcal{O}(y^3) \\ k &= 0.5(\overline{u^2} + \overline{v^2} + \overline{w^2}) \\ &= 0.5(\overline{a_1^2} + \overline{c_1^2}) + \mathcal{O}(y^3) \end{aligned} \tag{4.8}$$

The dissipation is defined as

$$\varepsilon = \nu \overline{\frac{\partial u_i}{\partial x_j} \frac{\partial u_i}{\partial x_j}} \tag{4.9}$$

Very close to the wall $\partial/\partial x$ and $\partial/\partial z$ terms are negligible. By using equation (4.7) the dissipation close to the wall can be rewritten as

$$\begin{aligned} \varepsilon &= \nu \left(\overline{\left(\frac{\partial u}{\partial y} \right)^2} + \overline{\left(\frac{\partial w}{\partial y} \right)^2} \right) \\ &= \nu \left(\overline{a_1^2} + \overline{c_1^2} \right) + \mathcal{O}(y) \end{aligned} \tag{4.10}$$

Equation (4.10) together with equation (4.8) give the new boundary condition for ε

$$\varepsilon \to 2\nu \frac{k}{y^2} \text{ as } y \to 0 \tag{4.11}$$

4.1.2 The standard $k-\omega$ model

The model was suggested by Wilcox [5] and is commonly referred to as the standard $k-\omega$ model. In addition to the k equation a new equation for the specific dissipation rate ω is derived to determine the turbulent length scale. The turbulent velocity scale is $k^{1/2}$ and time scale is $1/\omega$. The model equations read

$$U_j\frac{\partial k}{\partial x_j}=\frac{\partial}{\partial x_j}\left(\left(\nu+\frac{\nu_t}{\sigma_k}\right)\frac{\partial k}{\partial x_j}\right)+P_k-\beta^*\omega k \tag{4.12}$$

$$U_j\frac{\partial \omega}{\partial x_j}=\frac{\partial}{\partial x_j}\left(\left(\nu+\frac{\nu_t}{\sigma_\omega}\right)\frac{\partial \omega}{\partial x_j}\right)+\xi\frac{\omega}{k}P_k-\beta\omega^2 \tag{4.13}$$

The eddy viscosity is given by

$$\nu_t=\frac{k}{\omega} \tag{4.14}$$

The length scale is given by

$$l=\frac{k^{1/2}}{\omega} \tag{4.15}$$

The closure coefficients

$$\beta=0.075,\ \beta^*=0.09,\ \xi=\frac{5}{9},\ \sigma_k=2,\ \sigma_\omega=2$$

ω boundary condition

The boundary condition of ω is obtained by studying equation (4.13) in the near wall region where all the terms are negligible except the viscous diffusion and the dissipation terms.

$$\nu\frac{\partial^2\omega}{\partial y^2}-\beta\omega^2=0 \tag{4.16}$$

which directly gives

$$\omega_{wall}=\frac{6\nu}{\beta y^2} \tag{4.17}$$

4.2 $\overline{v^2}-f$ models

In the $\overline{v^2}-f$ model two new equations are solved together with the original equations of the two -equation model (k, and ε equation). These

new equations are $\overline{v^2}$ equation which represents the generic wall normal fluctuation component, and f equation. The first $\overline{v^2} - f$ model was originally suggested by Durbin [23]. In this model $\overline{v^2}^{1/2}$ is chose to be the turbulent velocity scale rather than $k^{1/2}$ as in the two-equation model. The model equations read (in addition to equation (4.1) and equation (4.2)).

$$U_j \frac{\partial \overline{v^2}}{\partial x_j} = \frac{\partial}{\partial x_j}\left(\left(\nu + \frac{\nu_t}{\sigma_k}\right)\frac{\partial \overline{v^2}}{\partial x_j}\right) + kf - \frac{\overline{v^2}}{k}\varepsilon \tag{4.18}$$

$$L^2 \frac{\partial^2 f}{\partial x_j^2} - f = \frac{C_1}{T}\left(\frac{\overline{v^2}}{k} - \frac{2}{3}\right) - C_2\frac{P_k}{k} - \frac{1}{T}\left(\frac{\overline{v^2}}{k} - \frac{2}{3}\right) \tag{4.19}$$

The eddy viscosity

$$\nu_t = C_\mu \overline{v^2} T \tag{4.20}$$

To avoid singularity problems near the wall (as $k \to 0$), Durbin suggested a lower boundary for the time and length scale by not letting them go down the Kolmogorov scales.
The time scale.

$$T = \max\left(\frac{k}{\varepsilon}, C_\zeta\sqrt{\frac{\nu}{\varepsilon}}\right) \tag{4.21}$$

The length scale

$$L = C_L \max\left(\frac{k^{3/2}}{\varepsilon}, C_\eta \frac{\nu^{3/4}}{\varepsilon^{1/4}}\right) \tag{4.22}$$

The closure coefficients

$$C_{\varepsilon 1} = 1.4\left(1 + a_1\sqrt{\frac{k}{\overline{v^2}}}\right)$$

$$C_{\varepsilon 2} = 1.9,\ C_\mu = 0.19,\ \sigma_\varepsilon = 1.3,\ \sigma_k = 1.0,\ C_1 = 1.4$$

$$C_2 = 0.3,\ C_L = 0.3,\ C_\eta = 70,\ C_\zeta = 6,\ a_1 = 0.045$$

f boundary condition

The boundary condition of f is derived by examining $\overline{v^2}$ equation in near wall region, which is of the form.

$$\nu \frac{\partial^2 \overline{v^2}}{\partial y^2} - \overline{v^2}\frac{\varepsilon}{k} + kf = 0 \tag{4.23}$$

Replacing k using equation (4.11), equation (4.23) is rewritten as

$$\frac{\partial^2\overline{v^2}}{\partial y^2} - 2\frac{v^2}{y^2} + \frac{\varepsilon f}{2\nu^2}y^2 = 0 \tag{4.24}$$

Very close to the wall f and ε are constant with respect to y. And the solution of equation (4.24) is

$$\overline{v^2} = Ay^2 + \frac{B}{y} - \varepsilon f\frac{y^4}{20\nu^2} \tag{4.25}$$

From the previous Taylor expansion we know that near the wall $\overline{v^2}$ behaves as $\mathcal{O}(y^4)$. To let $\overline{v^2}$ to have its right behavior, the constants A and B in equation (4.25) must equal zero. Hence, f boundary condition is

$$f = -\frac{20\nu^2\overline{v^2}}{\varepsilon y^4} \tag{4.26}$$

The strong coupling of f, $\overline{v^2}$ and ε in the wall boundary condition of f can make the model numerically unstable. Kalitzin [9] and Lien & Kalitzin [8] modified the model by deriving new boundary condition for f which makes the model more stable. In this thesis the $\overline{v^2}-f$ model given in Kalitzin [9] is used and it is described below.

4.2.1 $k-\varepsilon-\overline{v^2}-f$ model

In order to derive new boundary condition for f, we need to start by writing down the definition of kf

$$kf = \phi_{22} - \varepsilon_{22} + \frac{\overline{v^2}}{k}\varepsilon \tag{4.27}$$

According to Mansour et. al. [21] the behavior of ϕ_{22} and ε_{22} near walls is

$$\phi_{22} \to -2\frac{\overline{v^2}}{k}\varepsilon, \quad \varepsilon_{22} \to 4\frac{\overline{v^2}}{k}\varepsilon, \quad \text{as } y \to 0 \tag{4.28}$$

Inserting equation (4.28) in equation (4.27) yields

$$kf \to -2\frac{\overline{v^2}}{k}\varepsilon - 4\frac{\overline{v^2}}{k}\varepsilon + \frac{\overline{v^2}}{k}\varepsilon = -5\frac{\overline{v^2}}{k}\varepsilon \quad \text{as } y \to 0 \tag{4.29}$$

Equation (4.29) together with equation (4.11) give

$$f \to -5\frac{\overline{v^2}}{k}\varepsilon \to \frac{-20\nu^2\overline{v^2}}{\varepsilon y^4} \text{ as } y \to 0 \tag{4.30}$$

To enforce the behavior of kf near the wall to have the form of $kf \to 0$ as $y \to 0$, Lien and Kalitzin [8] added the term $\left(-5\overline{v^2}/k\right)\varepsilon$ to equation (4.27) and subtracted the same term from equation (4.18) in-order to maintain the balance. They also introduced a similar change in f equation to maintain the properties of the original model. The model equations as in Kalitzin [9] read

$$U_j\frac{\partial k}{\partial x_j} = \frac{\partial}{\partial x_j}\left(\left(\nu + \frac{\nu_t}{\sigma_k}\right)\frac{\partial k}{\partial x_j}\right) + P_k - \varepsilon \tag{4.31}$$

$$U_j\frac{\partial \varepsilon}{\partial x_j} = \frac{\partial}{\partial x_j}\left(\left(\nu + \frac{\nu_t}{\sigma_\varepsilon}\right)\frac{\partial \varepsilon}{\partial x_j}\right) + \frac{1}{T}\left(C_{\varepsilon 1}P_k - C_{\varepsilon 2}\varepsilon\right) \tag{4.32}$$

$$U_j\frac{\partial \overline{v^2}}{\partial x_j} = \frac{\partial}{\partial x_j}\left(\left(\nu + \frac{\nu_t}{\sigma_k}\right)\frac{\partial \overline{v^2}}{\partial x_j}\right) + kf - 6\overline{v^2}\frac{\varepsilon}{k} \tag{4.33}$$

$$L^2\frac{\partial^2 f}{\partial x_j^2} - f = \frac{C_1}{T}\left(\frac{\overline{v^2}}{k} - \frac{2}{3}\right) - C_2\frac{P_k}{k} - \frac{1}{T}\left(5\frac{\overline{v^2}}{k}\right) \tag{4.34}$$

The closure coefficients

$$C_{\varepsilon 2} = 1.9,\ C_\mu = 0.19,\ \sigma_\varepsilon = 1.3,\ \sigma_k = 1.0,\ C_1 = 0.4$$

$$C_2 = 0.3,\ C_L = 0.23,\ C_\eta = 70,\ C_\zeta = 6,\ a_1 = 0.045$$

4.2.2 Modified $\overline{v^2} - f$ model

Since $\overline{v^2}$ equation reduces the $\overline{v^2}$ as the walls are approached, $\overline{v^2}$ should be smaller than the other normal stresses . Hence $\overline{v^2}/k \leq 2/3$. In order to satisfy this condition, Davidson et. al. [19] suggested the modification described below.

In the original model far away from the wall $\overline{v^2}/k \geq 2/3$ and the main reason of this is that the Laplace term in f equation, namely $\partial^2 f/\partial y^2$, is not negligible in that region as it was assumed. One way to get around this problem is to set an upper bound on the source term kf in $\overline{v^2}$ equation as

$$\overline{v^2}_{source} = \min\left(kf,\ -\frac{1}{T}\left[\left(C_1 - 6\overline{v^2} - \frac{2}{3}k(C_1 - 1)\right] + C_2P_k\right)\right. \tag{4.35}$$

This modification had been applied on both $k - \varepsilon - \overline{v^2} - f$ model and $k - \omega - \overline{v^2} - f$ model and the results would be presented and discussed in the following chapter.

4.2.3 Formulation of $k-\omega-\overline{v^2}-f$ model

The main idea of this model is to solve the standard $k-\omega$ model along with the $\overline{v^2}-f$ model of Lien and Kalitzin [8]. The model equations are obtained simply by replacing the dissipation rate ε with the specific rate of dissipation ω. The model is described in the following section.

The specific rate of dissipation ω is connected to the dissipation rate ε through

$$\varepsilon = \beta^* \omega k \tag{4.36}$$

A modification is needed for the equations of which the dissipation rate ε is involved. Namely equation (4.33), equation (4.21) and equation (4.22). Inserting equation (4.36) in the mentioned equations yields

$$U_j \frac{\partial \overline{v^2}}{\partial x_j} = \frac{\partial}{\partial x_j}\left(\left(\nu + \frac{\nu_t}{\sigma_k}\right)\frac{\partial \overline{v^2}}{\partial x_j}\right) + kf - 6\overline{v^2}\beta^*\omega \tag{4.37}$$

The time scale

$$T = \max\left(\frac{1}{\beta^*\omega}, C_\zeta\sqrt{\frac{\nu}{\beta^*\omega k}}\right) \tag{4.38}$$

The length scale

$$L = C_L \max\left(\frac{k^{1/2}}{\beta^*\omega}, C_\eta \frac{\nu^{3/4}}{(\beta^*\omega k)^{1/4}}\right) \tag{4.39}$$

Finally the full set of $k-\omega-\overline{v^2}-f$ model equations read

$$U_j \frac{\partial k}{\partial x_j} = \frac{\partial}{\partial x_j}\left(\left(\nu + \frac{\nu_t}{\sigma_k}\right)\frac{\partial k}{\partial x_j}\right) + P_k - \beta^*\omega k \tag{4.40}$$

$$U_j \frac{\partial \omega}{\partial x_j} = \frac{\partial}{\partial x_j}\left(\left(\nu + \frac{\nu_t}{\sigma_\omega}\right)\frac{\partial \omega}{\partial x_j}\right) + \xi\frac{\omega}{k}P_k - \beta\omega^2 \tag{4.41}$$

$$U_j \frac{\partial \overline{v^2}}{\partial x_j} = \frac{\partial}{\partial x_j}\left(\left(\nu + \frac{\nu_t}{\sigma_k}\right)\frac{\partial \overline{v^2}}{\partial x_j}\right) + kf - 6\overline{v^2}\beta^*\omega \tag{4.42}$$

$$L^2\frac{\partial^2 f}{\partial x_j^2} - f = \frac{C_1}{T}\left(\frac{\overline{v^2}}{k} - \frac{2}{3}\right) - C_2\frac{P_k}{k} - \frac{1}{T}\left(6\frac{\overline{v^2}}{k} - \frac{2}{3}\right) \tag{4.43}$$

Determining the closure coefficients

C_μ constant

In the log-layer the most important terms in equation (4.40) are the production term and the dissipation term

$$\nu_t\left(\frac{\partial U}{\partial y}\right)^2 - \beta^*\omega k = 0 \tag{4.44}$$

In the log region the turbulent shear stress equal to the wall shear stress.

$$\left(\frac{\tau}{\rho}\right)_{wall} = -\overline{uv} = \nu_t \frac{\partial u}{\partial y} = u_*^2 \tag{4.45}$$

Using equation (4.45), equation (4.44) is rewritten as

$$u_*^4 = \nu_t \beta^* \omega k \tag{4.46}$$

Finally using equation (4.20) and equation (4.38), we rewrite equation (4.46) as

$$C_\mu = \left(\frac{u_*^2}{k}\right)^2 \frac{k}{\overline{v^2}} \tag{4.47}$$

It is well known from the experiments that in the log-law of the boundary layer $u_*^2/k \approx 0.3$, and from the DNS data of Moser et. al. [25] the value of $k/\overline{v^2}$ in the log region is found to be approximately 3. Hence $C_\mu = 0.27$.

The time and the length scales constants

In the literature the method of determining the time and the length scales constants C_ζ, C_L and C_η was not clear. Using the same constants value of the $k - \varepsilon - \overline{v^2} - f$ model showed that the shifting from Kolmogorov scales to the normal scales took place far away from the wall. The constants were re-tuned to achieve the scales shifting at the same value of y^+ as in $k - \varepsilon - \overline{v^2} - f$ (at $y^+ = 5$ for the time scale and at $y^+ = 35$ for the length scale). The value of the new constants is found to be

$$C_L = 0.5,\ C_\eta = 15,\ \ C_\zeta = 0.5$$

ω Prandtl Number (σ_ω)

Choosing $\sigma_\omega = 2$ as in the standard $k - \omega$ model moves the peak of ω and consequently ε away from the wall and results in poor prediction of the mean velocity profile. The constant is re-tuned to get the best fit with the DNS data [25]. The constant value is found to be $\sigma_\omega = 1$.

The rest of constants are unchanged. The model constants are given in the table below, the method of obtaining each constant is also included.

The Coefficient	Value	Method of determining the coefficient
β^*	0.09	standard
β	0.075	standard
ξ	5/9	standard
C_1	1.4	standard
C_2	0.3	standard
σ_k	2.0	standard
σ_ω	1.0	modified
C_μ	0.27	calculated using the DNS data
C_L	0.5	modified
C_η	1.5	modified
C_ζ	0.5	modified

4.3 The performance of the $\overline{v^2}-f$ models in channel flow

The performance of four $\overline{v^2}-f$ models – the $k-\varepsilon-\overline{v^2}-f$, the modified $k-\varepsilon-\overline{v^2}-f$, the $k-\omega-\overline{v^2}-f$, and the modified $k-\omega-\overline{v^2}-f$ – is examined in fully developed channel flow. The Reynolds number based on the friction velocity is $Re_\tau = 395$. The number of control volumes used to cover half of the channel is 64, and a geometric stretching factor of 1.08 is used. The results are compared to the DNS data $Re_\tau = 395$ [25].

Figure (4.1(a)) shows the predicted mean velocity. It is clear that all models over-predict the mean velocity after $y^+ = 40$. This mainly could be associated with the under-prediction of the eddy viscosity in the same region as shown in figure (4.1(g)). The modified $k-\omega-\overline{v^2}-f$ model continues to over-predict the mean velocity after $y^+ = 200$ for values even higher than the other models due to it is small value of the eddy viscosity. For all models, the higher values of the eddy viscosity is balanced by the low values of the mean velocity gradients result in a good prediction of the Reynolds shear stress, figure (4.1(c)), with exception of the $k-\omega-\overline{v^2}-f$ and the modified $k-\omega-\overline{v^2}-f$ where the $\overline{uv}$ is under-predicted for $5 \leq y^+ \leq 50$. From figure (4.1(e)) it can be seen that the turbulent kinetic energy is over-predicted by the $k-\varepsilon-\overline{v^2}-f$ and the modified $k-\varepsilon-\overline{v^2}-f$, while it is under-predicted by the $k-\varepsilon-\overline{v^2}-f$ and the modified $k-\varepsilon-\overline{v^2}-f$. This mismatch is balanced by the prediction of $\overline{v^2}$, figure (4.1(f)), in the eddy viscosity expression, equation (4.20).

The performance of the models is also analyzed for a higher Reynolds number, $Re_\tau = 6000$. The results are shown in figure (4.2). These re-

sults are shown to have the same trend of the previous results, which confirms the consistency of the $k - \omega - \overline{v^2} - f$ model.

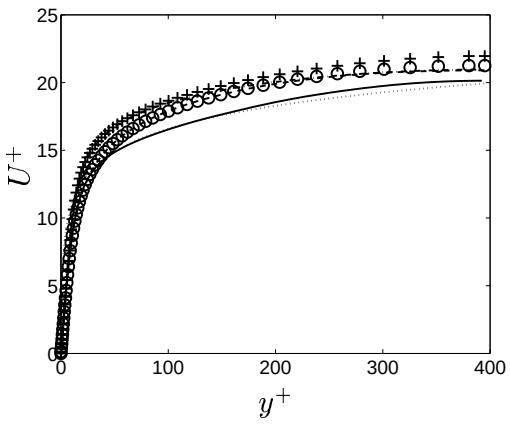

(a) U^+

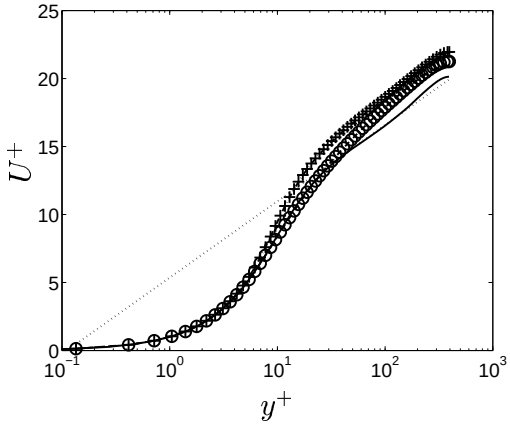

(b) U^+

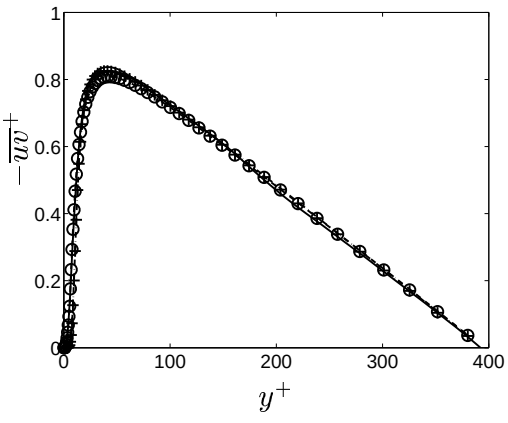

(c) $-\overline{uv}^+$

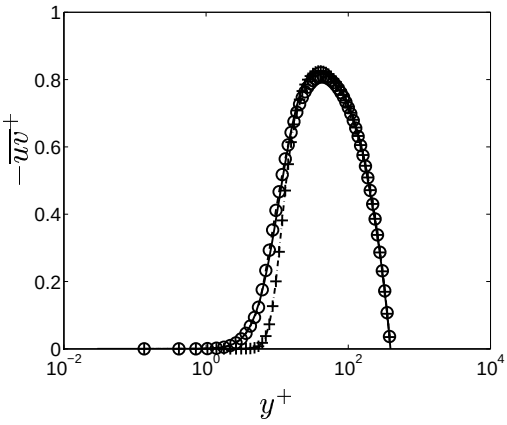

(d) $-\overline{uv}^+$

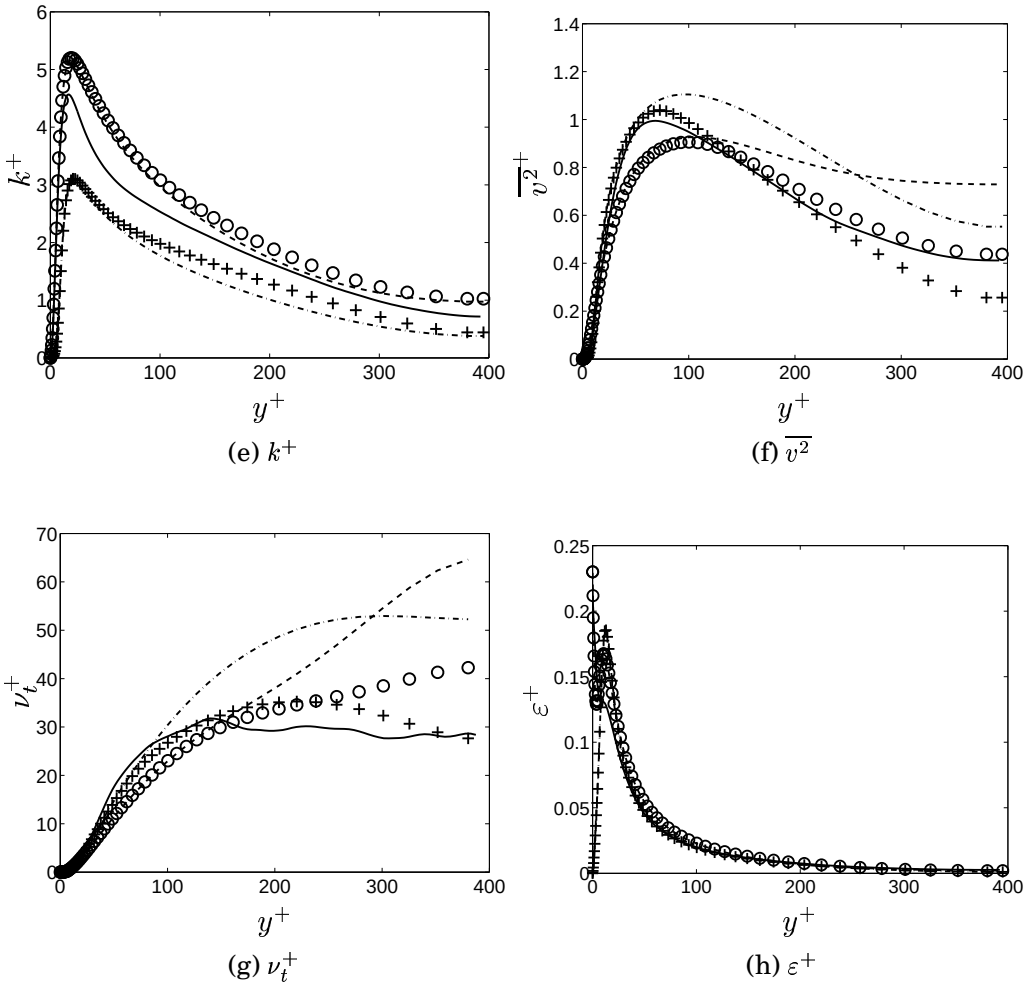

(e) k^+ (f) $\overline{v^2}$

(g) ν_t^+ (h) ε^+

Figure 4.1: Turbulent quantities of fully developed channel flow compared to the DNS data $Re_\tau = 395$. Solid line: DNS data; dotted line: Log law; dashed dotted line: $k - \omega - \overline{v^2} - f$; dashed line: $k - \varepsilon - \overline{v^2} - f$; $+$: modified $k - \omega - \overline{v^2} - f$; $\circ$: modified $k - \varepsilon - \overline{v^2} - f$.

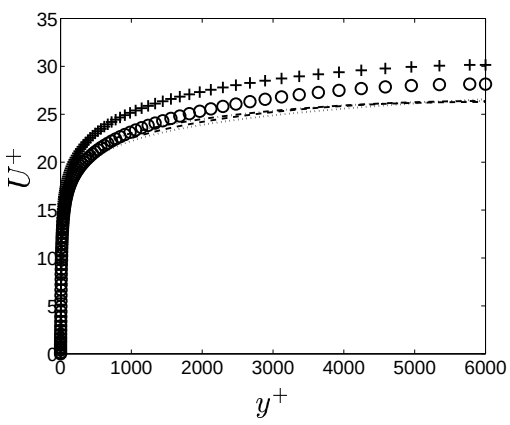

(a) U^+

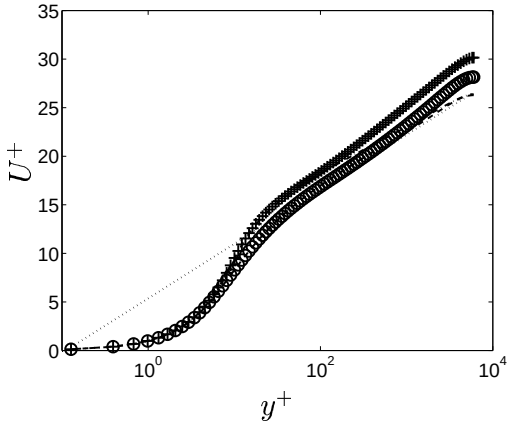

(b) U^+

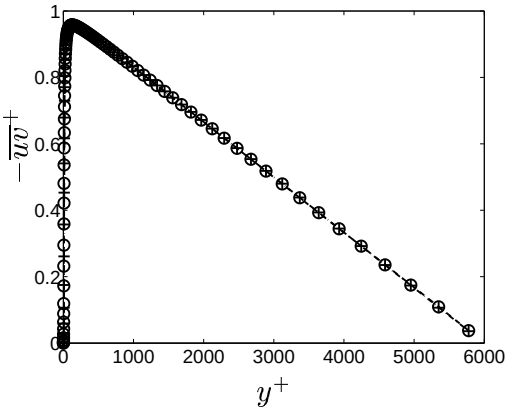

(c) $-\overline{uv}^+$

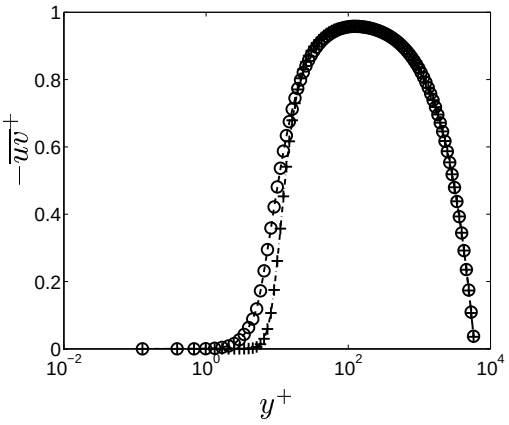

(d) $-\overline{uv}^+$

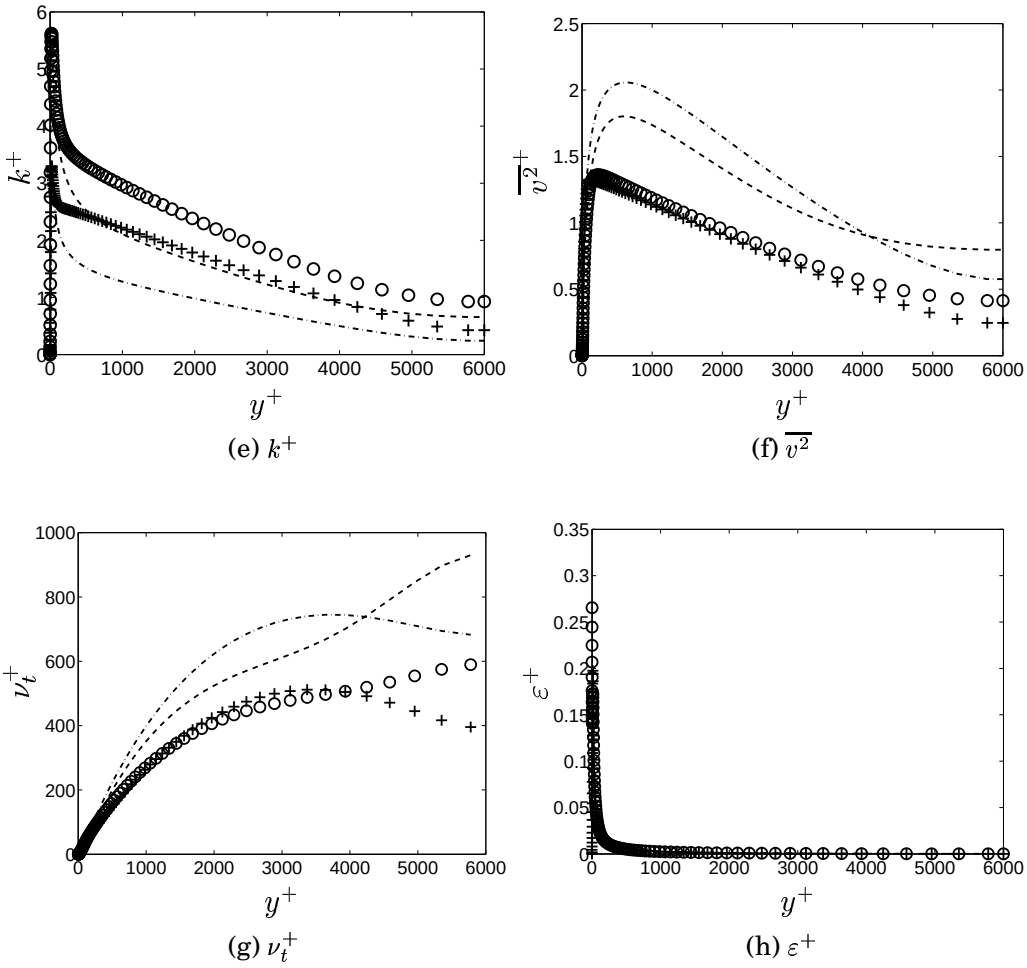

(e) k^+ (f) $\overline{v^2}$

(g) ν_t^+ (h) ε^+

Figure 4.2: Turbulent quantities of fully developed channel flow $Re_\tau = 6000$. Dotted line: Log law; dashed dotted line: $k-\omega-\overline{v^2}-f$; dashed line: $k-\varepsilon-\overline{v^2}-f$; +: modified $k-\omega-\overline{v^2}-f$; ∘: modified $k-\varepsilon-\overline{v^2}-f$.

Chapter 5

Results

No doubts that the validation of turbulence models plays a key role as the final quality control mechanism. It is impossible to assess the validity of the models or the accuracy of its final results by any means other than a comparison with experimental data. Validation of turbulence models requires detailed information concerning the boundary conditions of a test case and generates a large volume of results. To validate the models in a meaningful way it is necessary to produce experimental data of similar scope to compare with.

In the previous chapter the performance of the $k-\omega-\overline{v^2}-f$ model in 1D fully developed flow was assessed. However the model requires additional testing since the model is intended for computing complex engineering flows. In the this chapter the results of numerical simulations of a well documented separated flow in asymmetric plane diffuser will be presented and discussed.

5.1 Experimental Test Case

The experimental test case presented in this thesis is a separated flow in an asymmetric plane diffuser. This flow is of considerable interest to turbulence modelers due to it is simple geometry and the availability of two sets of experimental data [22] [2]. The flow has several desirable features which make it good test case for validation. According to Kaltenbrach [12] the most important features are:

- The flow experiences pressure-driven separation from a smooth wall. Many technical devices are designed to operate under these conditions .
- The flow exhibits rich flow physics, such as the combined effects of adverse pressure gradient and convex curvature near the diffuser

inlet.

- The inlet duct has a length of more than 100 duct heights, thereby guaranteeing that the inlet flow is fully developed turbulent channel flow.

In such flow, determining the separation line depends on the correct modeling of the shear stress and normal stresses, while the reattachment point mainly depends on the magnitude of the shear stress in a free shear layer. The major challenges of turbulence models in such a flow are:

- To predict the correct time scale.
- To predict the correct anisotropy of the Reynold stress tensor.

The test case geometry is shown in figure 5.1. The geometry is divided into three regions: the inlet, the diffusing section and the outlet. The diffusing section has a length $21H$, where H is the inlet channel height, and an overall expansion ratio of 4.7. The inlet plane is located at $x/H = -5$ and the exit plane is located at $x/H = 75$. The Reynolds number based on the bulk velocity U_b at the inlet section and H is $Re_b = 18000$, which matches the experimental configuration. The corresponding Reynolds number based on the friction velocity u_* is $Re_\tau = 500$.

Obi et. al. [22] investigated the flow using two component laser Doppler anemometry (LDA) in a wind tunnel. The aspect ratio of the configuration was $1:35$ while for the outflow it was $1:7.4$ which is not sufficient to ensure two-dimensional flow. They measured mean velocity profiles and Reynolds stresses at stations between $x/H = 3.2$ and $x/H = 25.2$. The pressure was only measured along the flat wall. The same experiment was repeated by Buice & Eaton [2] with careful attention to eliminate the side wall effects. The pressure level in the facility was raised through the exit blockage in order to control the sidewall boundary layer leakage. The velocity was measured with hot-wire technique. They were unable to obtain measurements in the recirculating flow. However, they extend the coverage of flow development downstream, and added skin-friction coefficients and surface pressure on the inclined wall to the data set.

The flow was reported to separate from the inclined wall at $x/H = 7.5$ and to reattach at $x/H = 29$.

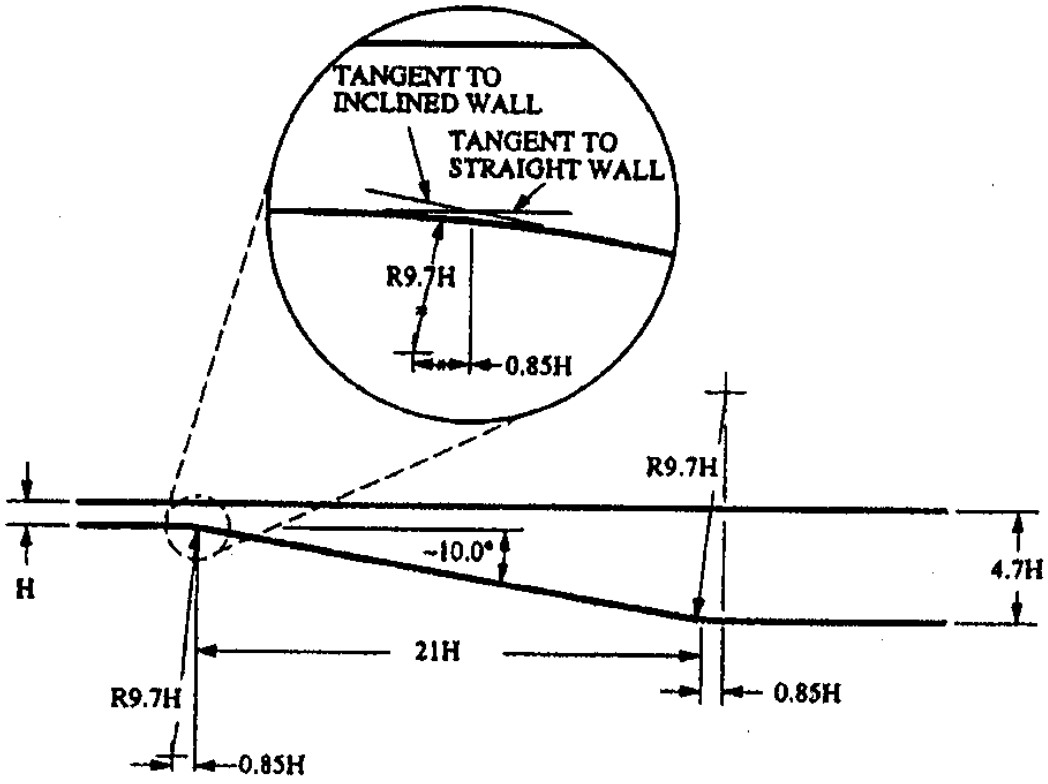

Figure 5.1: The computational domain

5.2 Computational Domain

The computational domain is the asymmetric plane diffuser of Obi et. al. [22] (figure 5.1). The domain extended from $x/H = -11$ to $x/H = 60$. The mesh was generated using FORTRAN program by D.D Apsley [6] specially written for the asymmetric plane diffuser. Mesh size of 280 x 120 control volumes is employed. The near wall grid sizes were chosen to obtain $y^+ = 1$ at the cell centers.

5.3 Boundary Conditions

Inlet and outlet boundary condition

It is more reliable to obtain the inlet boundary conditions from the experimental data. However, sometimes it is experimentally rather difficult to obtain the profiles of some turbulent quantities such as ε

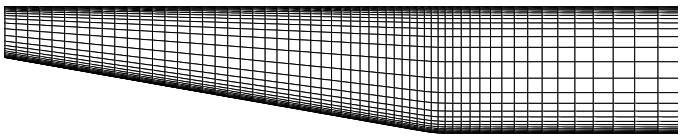

Figure 5.2: The diffuser mesh

and ω. Due to such difficulties, another approach was used in this thesis to obtain the inlet boundary condition.

As mentioned before, the diffuser inlet section was long enough to ensure fully developed turbulent flow at the inlet, hence the inlet boundary condition was obtained by computing a fully developed channel flow of $Re_\tau = 500$ using the same turbulence model that will be used of the diffuser computations.

At the outlet the Neumann condition was used for all variables.

Wall boundary condition

Due to the no-slip condition on the wall, the wall boundary condition of the velocity components and the turbulent kinetic energy.

$$U = V = W = k = 0$$

The wall boundary condition of the remaining parameters is.

$$\varepsilon_{wall} = \nu \frac{2k}{y^2}$$

$$\omega_{wall} = \nu \frac{6}{\beta y^2}$$

$$f = 0$$

5.4 Grid Independence

The grid independence is studied for the $k-\varepsilon-\overline{v^2}-f$ model and the $k-\omega-\overline{v^2}-f$ model employing two types of grids with different values of y^+ to examine the sensitivity of ε and ω boundary conditions.

- Coarse mesh 280 x 60 with $y^+ = 1$.
- Fine mesh 280 x 120 with $y^+ = 1$.
- Fine mesh 280 x 120 with $y^+ = 2$.
- Fine mesh 280 x 120 with $y^+ = 5$.
- Fine mesh 280 x 120 with $y^+ = 0.5$.

In addition, the effect of the inlet boundary condition is also studied by employing the DNS data of fully developed channel flow ($Re_\tau = 500$) of Moser et. al. [25] as inlet condition. In all computations, the van leer scheme was used due to its higher order accuracy. The effect of the differencing scheme is also investigated in terms of the Hybrid scheme. For the modified $k - \varepsilon - \overline{v^2} - f$ and the modified $k - \omega - \overline{v^2} - f$, only the first two types of mesh are studied.

Figures 5.3(a), 5.3(b), 5.4(a) and 5.4(b) show the mean velocity profile and the Reynolds shear stress computed by the $k-\varepsilon-\overline{v^2}-f$ and the modified $k-\varepsilon-\overline{v^2}-f$ respectively. And figures 5.5(a), 5.5(b), 5.6(a) and 5.6(b) show the same parameters computed by the $k - \omega - \overline{v^2} - f$ and the modified $k-\omega-\overline{v^2}-f$ respectively. All the obtained quantities are plotted in the middle of the diffusing section (after the separation point and beyond the reattachment point at $x/H = 8$). The results showed that the adopted grid for both models was sufficient for the numerical accuracy. This is also confirmed by the results of Hybrid scheme. A large deviation was observed when employing 280 x 120 control volumes with $y^+ = 5$, and no separation was detected. This is mainly because the boundary conditions are assigned on the edge of the viscous layer. The results also showed that the $k-\varepsilon-\overline{v^2}-f$ model is not sensitive to the inlet boundary condition while the $k-\omega-\overline{v^2}-f$ is highly sensitive.

It was concluded from the mesh dependence study that the $k - \omega - \overline{v^2} - f$ model is highly sensitive to the inlet boundary condition. Figure 5.7 illustrates the difference between the the different boundary conditions used in the computations.

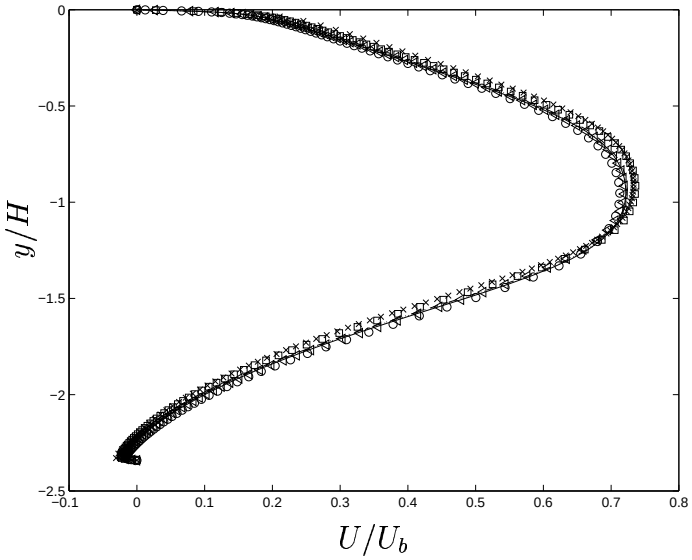

(a) Mean velocity profile

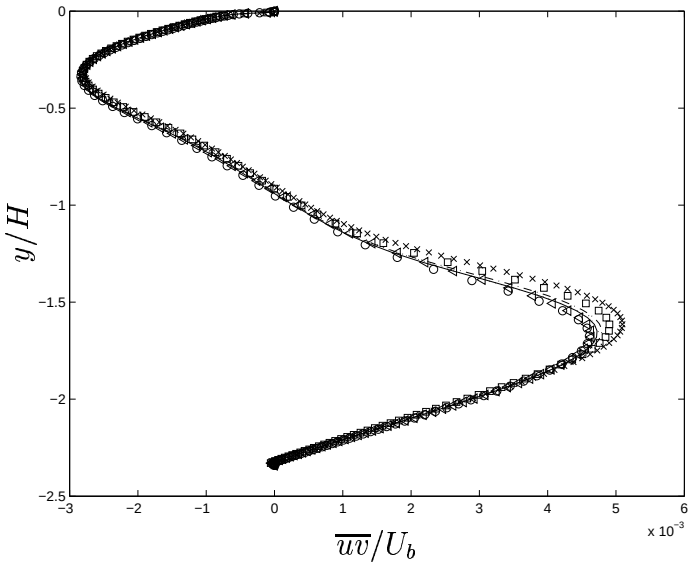

(b) Reynolds shear stress

Figure 5.3: Mean velocity profile and Reynolds shear stress at $x/H = 8$ computed by the $k-\varepsilon-\overline{v^2}-f$ model. Dotted line: 280x60 $y^+ = 1$; solid line: 280x120 $y^+ = 1$; dashed line: 280x120 $y^+ = 2$; x: 280x120 $y^+ = 5$; $\circ$: 280x120 $y^+ = 0.5$; $\square$: 280x120 $y^+ = 1$ – DNS inlet B.C; $\triangleleft$: 280x60 $y^+ = 1$ Hybrid scheme.

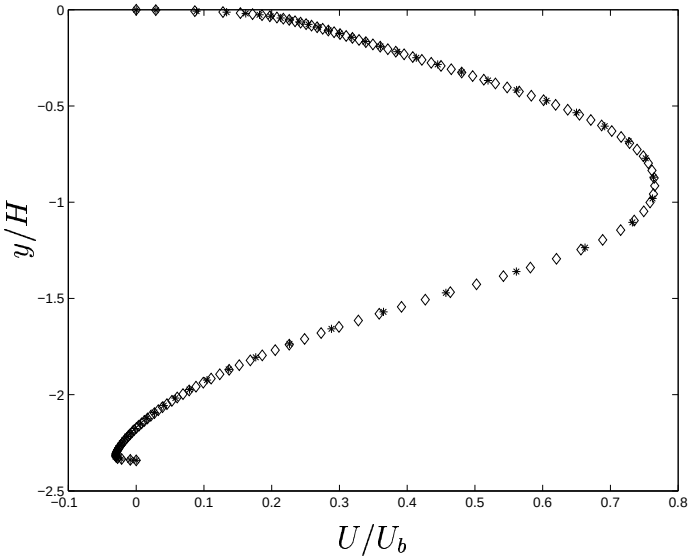

(a) Mean velocity profile

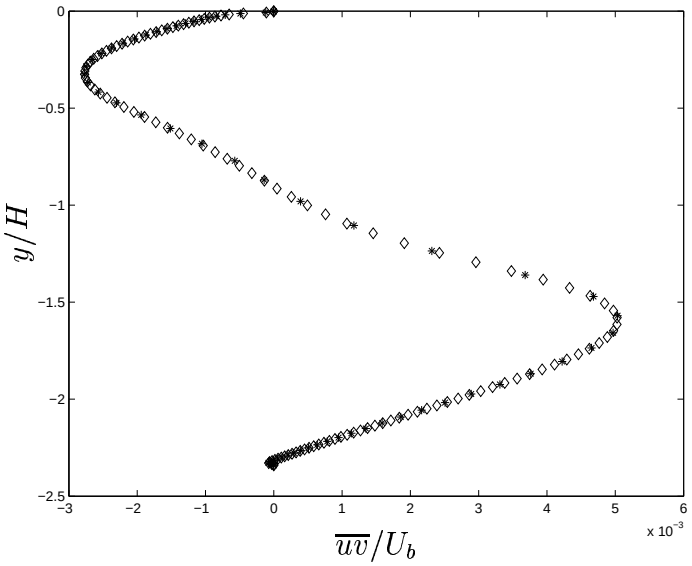

(b) Reynolds shear stress

Figure 5.4: Mean velocity profile and Reynolds shear stress at $x/H = 8$ computed by the modified $k - \omega - \overline{v^2} - f$ model. $*$: 280x60 $y^+ = 1$; $\diamond$: 280x120 $y^+ = 1$.

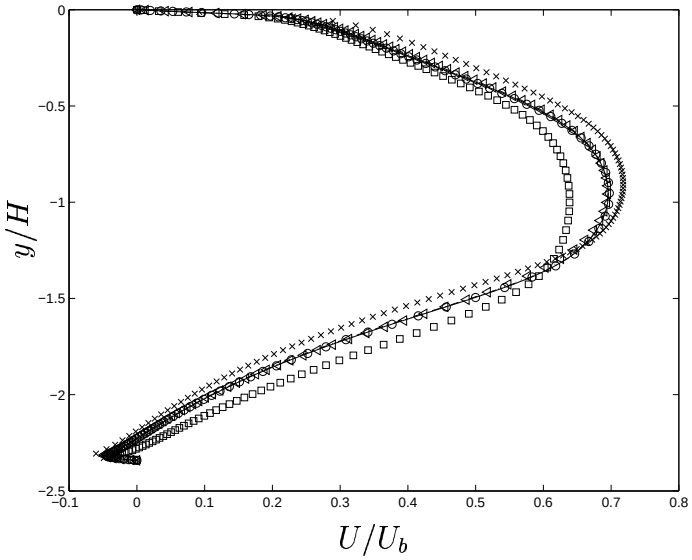

(a) Mean velocity profile

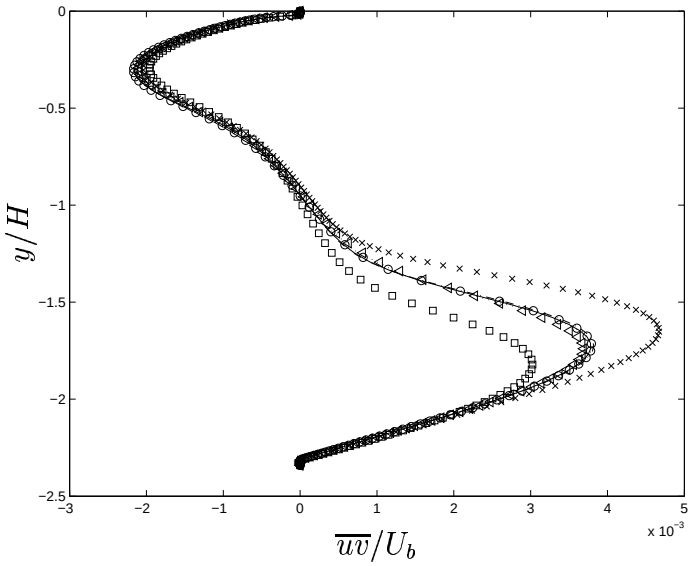

(b) Reynolds shear stress

Figure 5.5: Mean velocity profile and Reynolds shear stress at $x/H = 8$ computed by the $k-\omega-\overline{v^2}-f$ model. Dotted line: 280x60 $y^+ = 1$; solid line: 280x120 $y^+ = 1$; dashed line: 280x120 $y^+ = 2$; x: 280x120 $y^+ = 5$; $\circ$: 280x120 $y^+ = 0.5$; $\square$: 280x120 $y^+ = 1$ – DNS inlet B.C; $\triangleleft$: 280x60 $y^+ = 1$ Hybrid scheme.

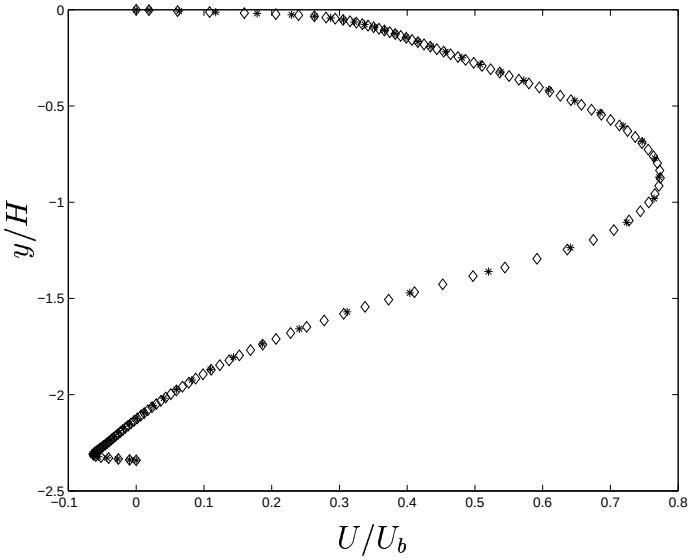

(a) Mean velocity profile

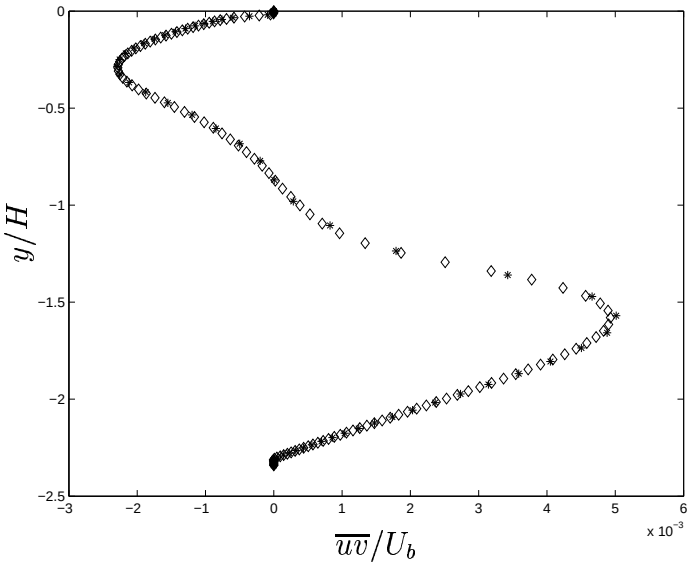

(b) Reynolds shear stress

Figure 5.6: Mean velocity profile and Reynolds shear stress at $x/H = 8$ computed by the modified $k - \omega - \overline{v^2} - f$ model. $*$: 280x60 $y^+ = 1$; $\diamond$: 280x120 $y^+ = 1$.

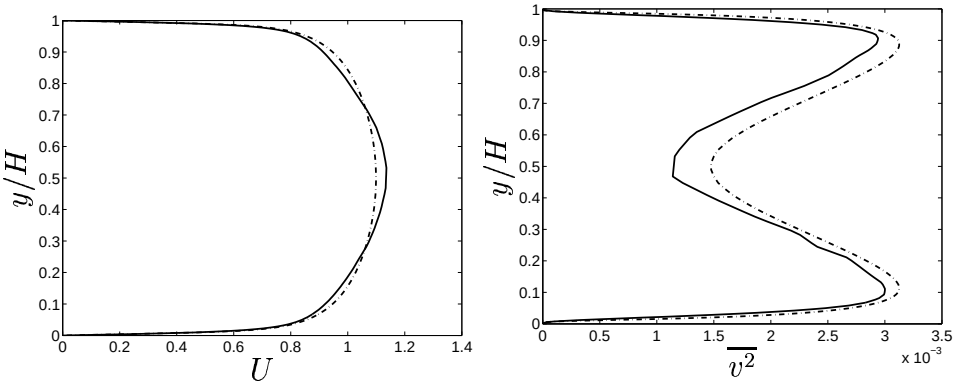

(a) U (b) $\overline{v^2}$

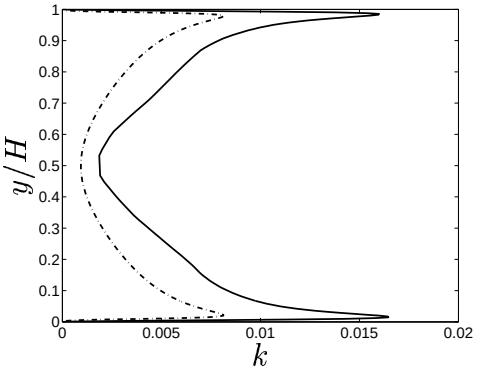

(c) k

Figure 5.7: Comparison of different inlet boundary conditions. Solid line: DNS data ($Re_\tau = 500$); dashed line: fully developed channel flow computed by the $k-\omega-\overline{v^2}-f$ model.

5.5 Results and Discussions

The results of the $k-\varepsilon-\overline{v^2}-f$, the modified $k-\varepsilon-\overline{v^2}-f$, the $k-\omega-\overline{v^2}-f$, and the modified $k-\omega-\overline{v^2}-f$ are plotted together with the experimental data and presented in this section. It is organized as follows. First the results of the $k-\varepsilon-\overline{v^2}-f$ and the modified $k-\varepsilon-\overline{v^2}-f$ will be presented and discussed, then the results of the $k-\omega-\overline{v^2}-f$ and the modified $k-\omega-\overline{v^2}-f$.

5.5.1 $k-\varepsilon-\overline{v^2}-f$ Model

Figures 5.8(a) and 5.8(b) show the mean velocity profile along the diffuser. In the recirculating region, the velocity was very good predicted with the the $k-\varepsilon-\overline{v^2}-f$ model, while it was over predicted by the modified $k-\varepsilon-\overline{v^2}-f$ model. However both models over-predict the velocity after the reattachment point. As indicated earlier, the prediction of separation point depends on the proper prediction of Reynolds stresses. Figures 5.9(a), 5.9(b), 5.10(a), 5.10(b), 5.11(a) and 5.11(b) show the Reynolds stresses $\overline{uu}$, $\overline{vv}$ and $\overline{uv}$ respectively. A peak for all the stresses was found in the center region due to the adverse pressure gradient. The stresses predicted with both models are shown to be in a good agreement with the experimental data. The pressure coefficient C_p on the plane wall is presented in figure 5.12(a). This parameter reflects the shape of the recirculating region. It is clear that the depth of the recirculating flow is much better predicted with the $k-\varepsilon-\overline{v^2}-f$ model. The skin-friction coefficient C_f is presented in figure 5.12(b). It is an important parameter to indicate the separation and reattachment points. The recirculating region is identified by the negative values of C_f. The separation was captured by both models. Again the $k-\varepsilon-\overline{v^2}-f$ model was able to predict the separation and reattachment points very close to the experiment.

5.5.2 $k-\omega-\overline{v^2}-f$ Model

The mean velocity profile is shown in figure 5.13(a) and figure 5.13(b). The results of the $k-\omega-\overline{v^2}-f$ fairly agree with the experiment especially in the recirculating region, while over-prediction of the velocity was recorded when employing the modified $k-\omega-\overline{v^2}-f$ (this is consistent with the previous results of the channel flow). Figures 5.14(a), 5.14(b), 5.15(a), 5.15(b), 5.16(a) and 5.16(b) represent the Reynolds stresses $\overline{uu}$, $\overline{vv}$ and $\overline{uv}$ respectively. The stresses are fairly well predicted with both models. However, the modified $k-\omega-\overline{v^2}-f$ showed

The Model	Separation point x_S/H	Reattachment point x_R/H
$k-\varepsilon-\overline{v^2}-f$	5	29
Modified $k-\varepsilon-\overline{v^2}-f$	4.5	30
$k-\omega-\overline{v^2}-f$	3	28
Modified $k-\omega-\overline{v^2}-f$	2.5	29

Table 5.1: Summary of separation point and reattachment point.

a moderate degree of over-prediction of $\overline{vv}$ and $\overline{uv}$. The pressure coefficient C_p presented in figure 5.17(a) revealed that the depth of the recirculating region is much better predicted by the $k-\omega-\overline{v^2}-f$. Both models captured the separation as it is shown in figure 5.17(b). The models predicted the separation point too early, on the other hand the prediction of reattachment point agrees well with the experiment. An interesting feature is observed in the results of both models. They predict a tiny region of recirculation right at the corner (at the inlet to the diffusing section), the same feature also revealed by the LES data [20], although both experimental data were not able to clarify this.

The performance of the four models in terms of the separation point and reattachment point is summarized in the table 5.1.

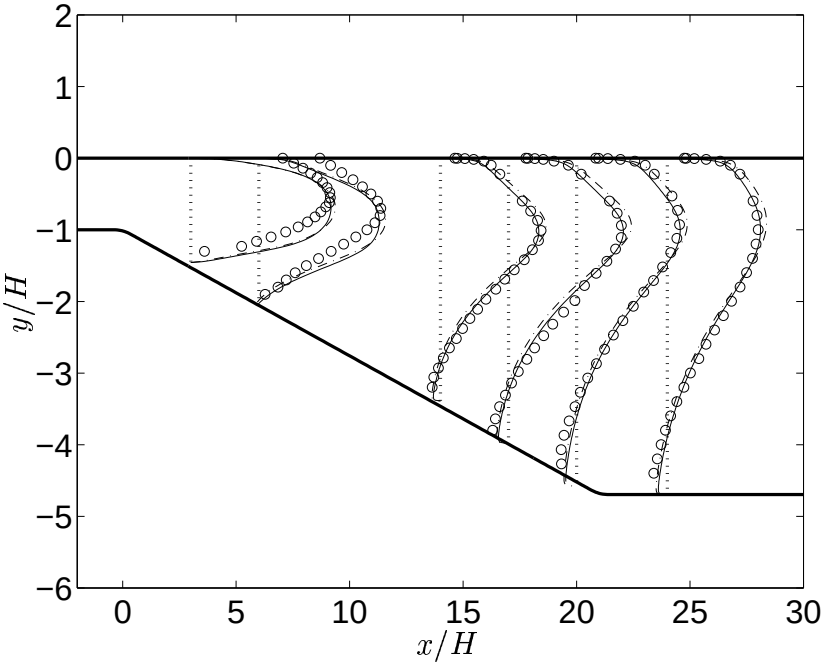

(a) Mean velocity profile

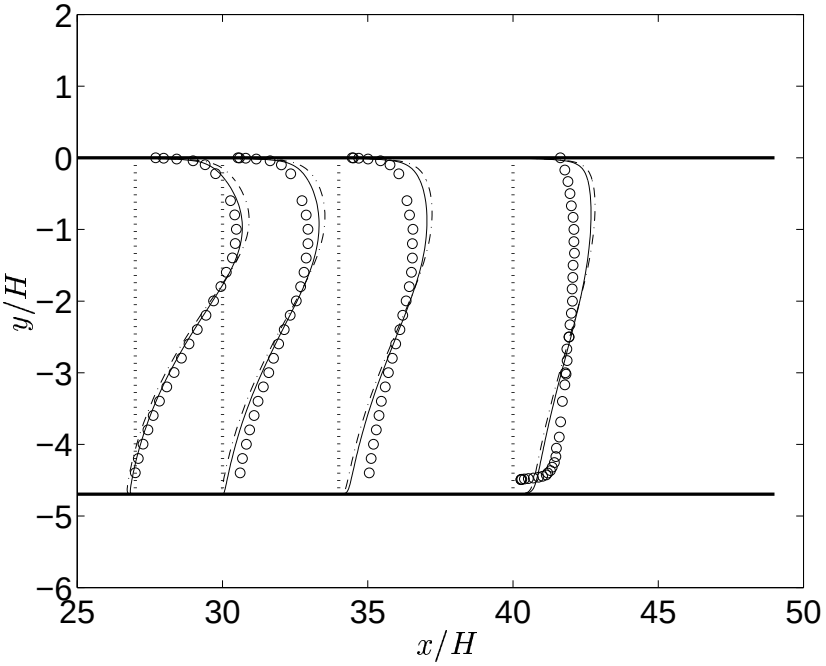

(b) Mean velocity profile

Figure 5.8: Mean velocity profile. Solid line: $k-\varepsilon-\overline{v^2}-f$; dashed line: modified $k-\varepsilon-\overline{v^2}-f$; $\circ$: experimental data [2].

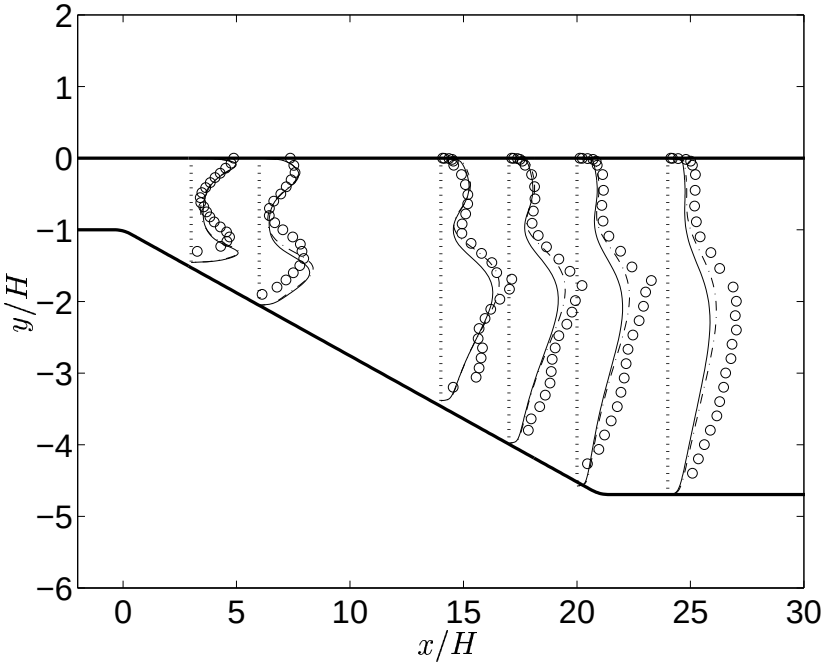

(a) Reynolds stress $\overline{uu}$

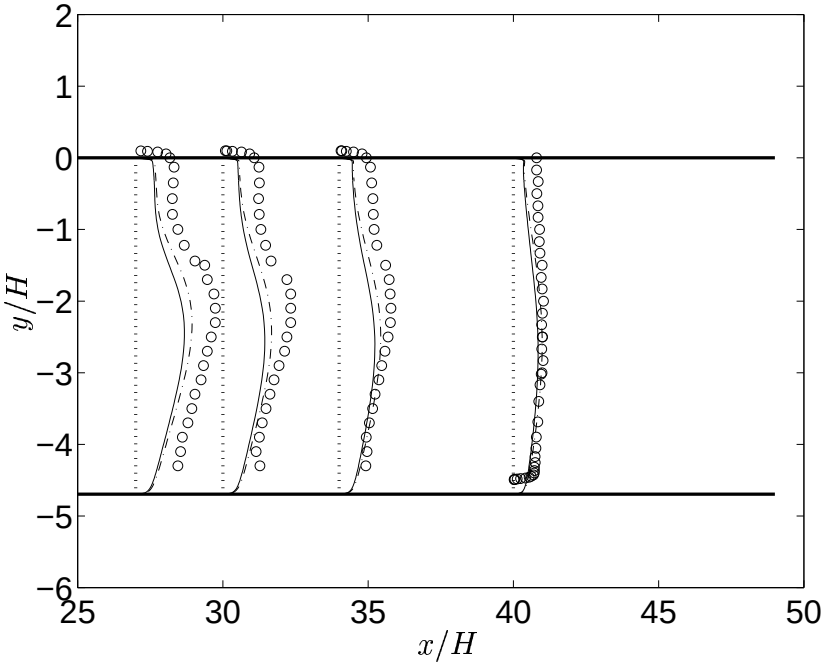

(b) Reynolds stress $\overline{uu}$

Figure 5.9: Reynolds stress $\overline{uu}$. Solid line: $k-\varepsilon-\overline{v^2}-f$; dashed line: modified $k-\varepsilon-\overline{v^2}-f$; $\circ$: experimental data [2].

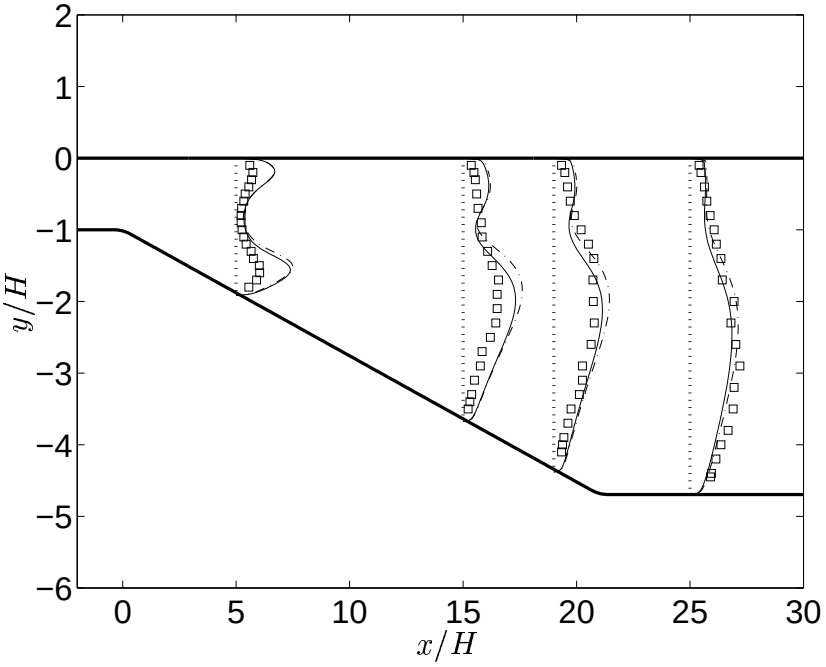

(a) Reynolds stress $\overline{vv}$

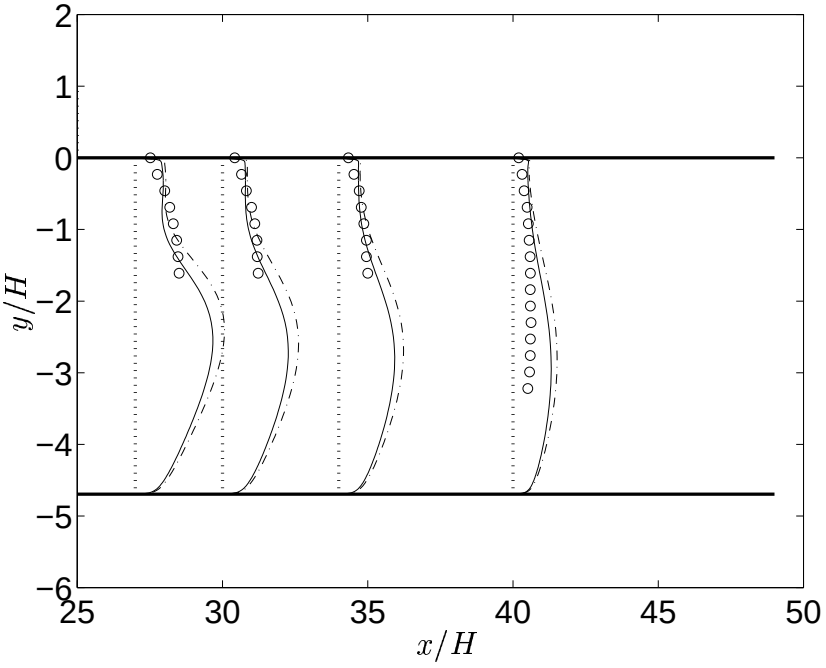

(b) Reynolds stress $\overline{vv}$

Figure 5.10: Reynolds stress $\overline{vv}$. Solid line: $k-\varepsilon-\overline{v^2}-f$; dashed line: modified $k-\varepsilon-\overline{v^2}-f$; ∘: experimental data [2]; □: experimental data [22].

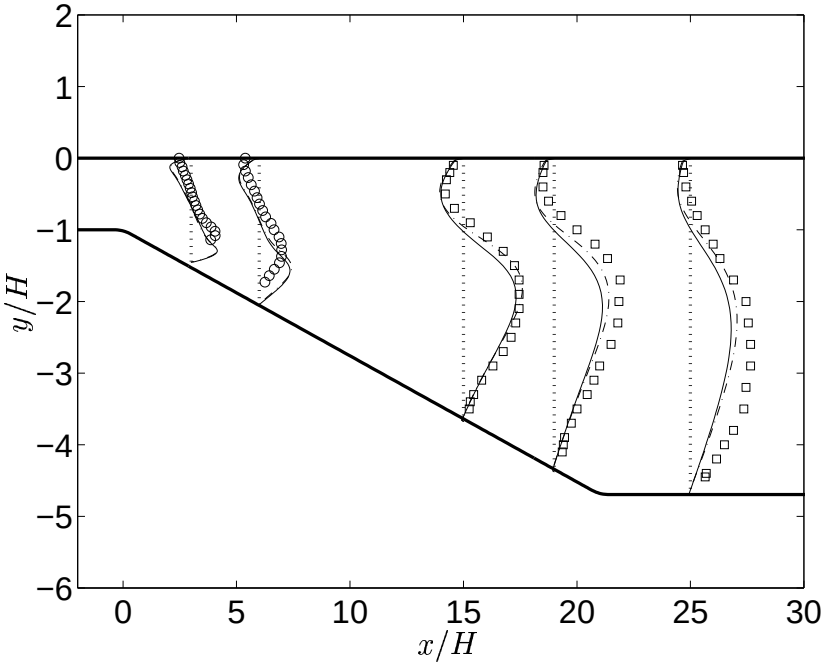

(a) Reynolds shear stress $\overline{uv}$

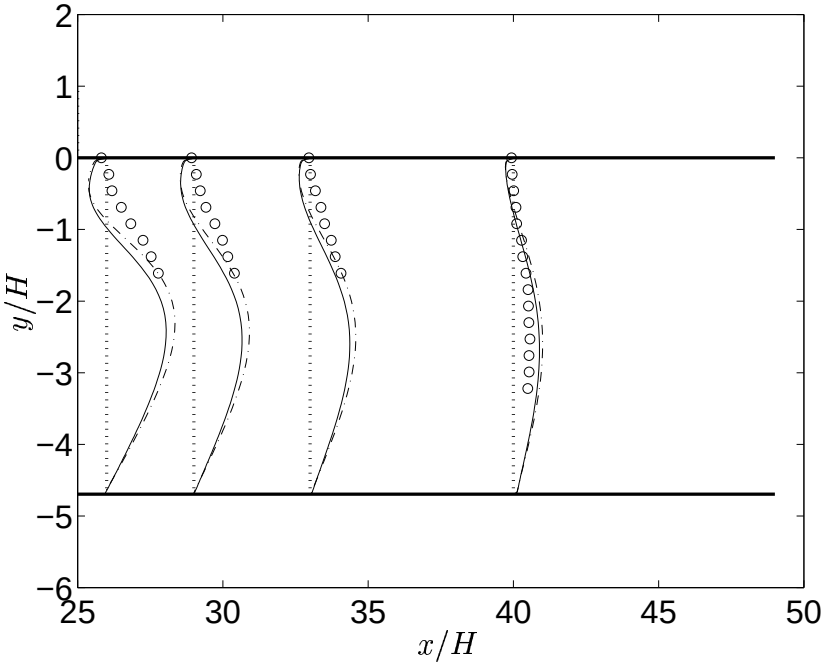

(b) Reynolds shear stress $\overline{uv}$

Figure 5.11: Reynold shear stress $\overline{uv}$. Solid line: $k-\varepsilon-\overline{v^2}-f$; dashed line: modified $k-\varepsilon-\overline{v^2}-f$; ∘: experimental data [2]; □: experimental data [22].

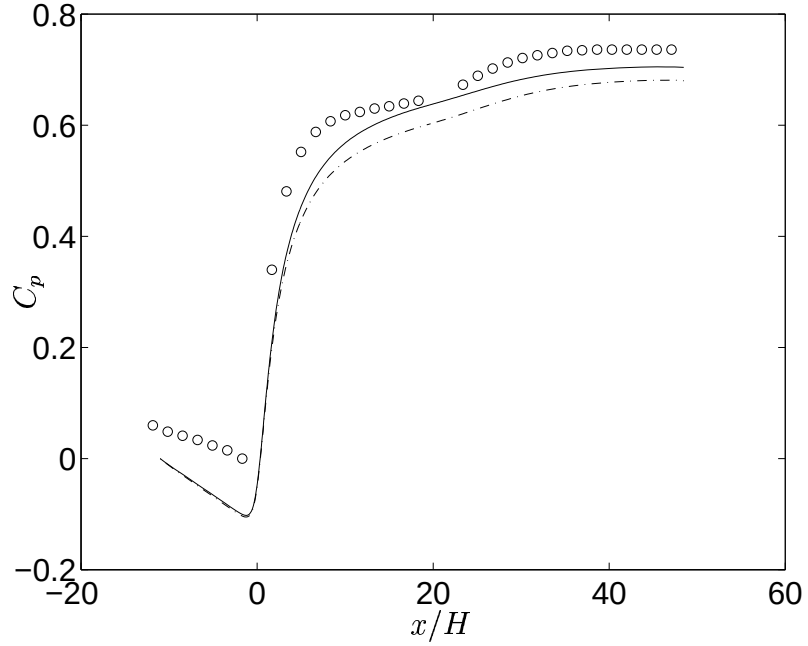

(a) The pressure coefficient C_p

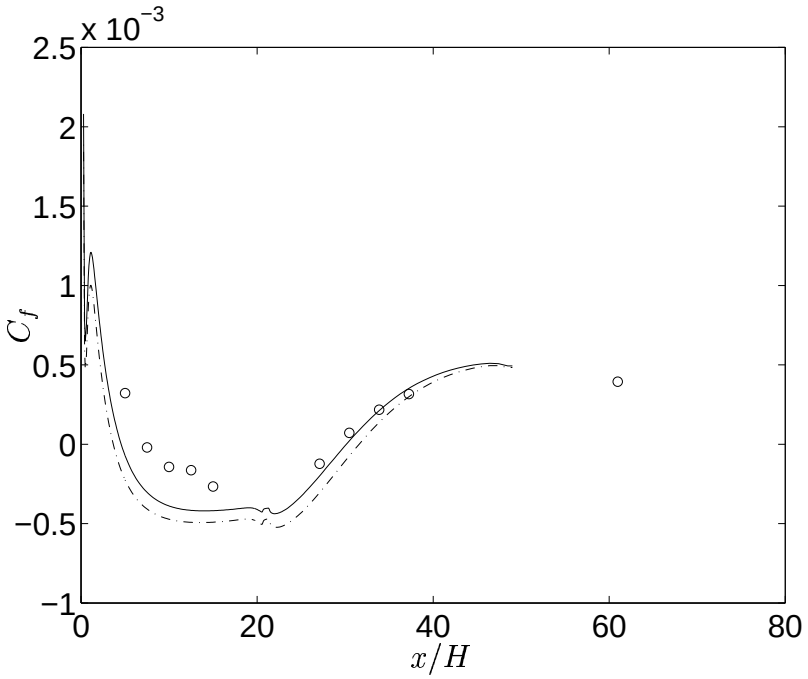

(b) The skin friction coefficient C_f

Figure 5.12: Pressure coefficient and skin-friction. Solid line: $k-\varepsilon-\overline{v^2}-f$; dashed line: modified $k-\varepsilon-\overline{v^2}-f$; $\circ$: experimental data [2].

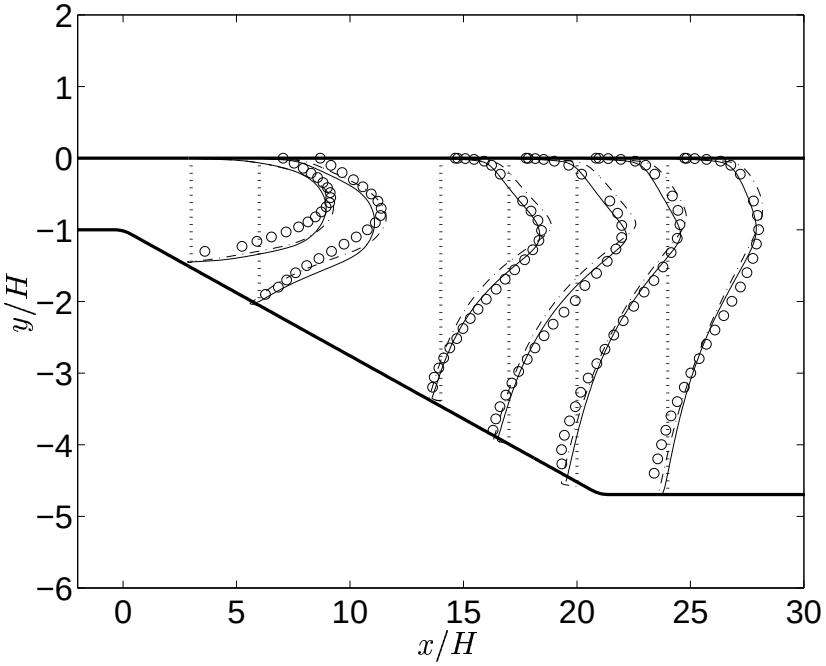

(a) Mean velocity profile

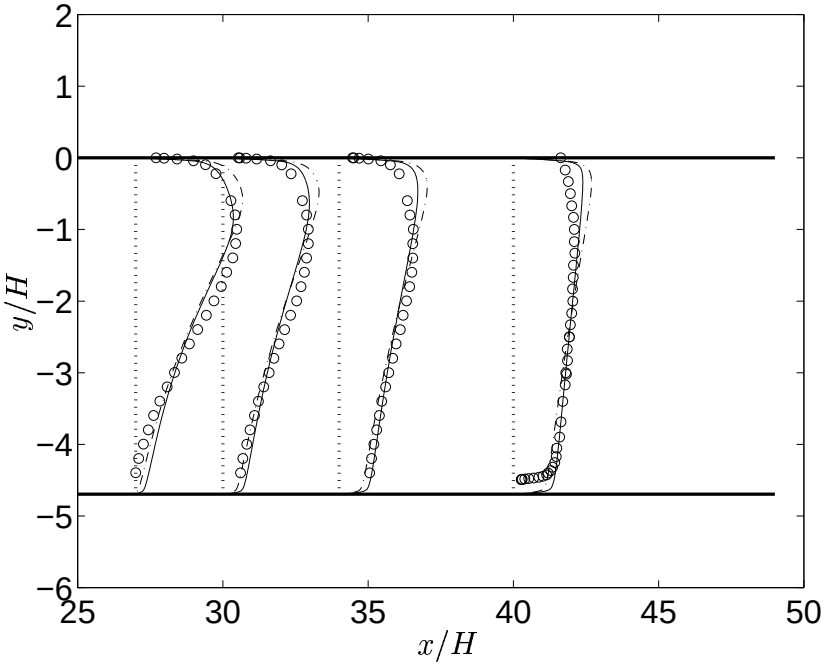

(b) Mean velocity profile

Figure 5.13: Mean velocity profile. Solid line: $k-\omega-\overline{v^2}-f$; dashed line: modified $k-\omega-\overline{v^2}-f$; $\circ$: experimental data [2].

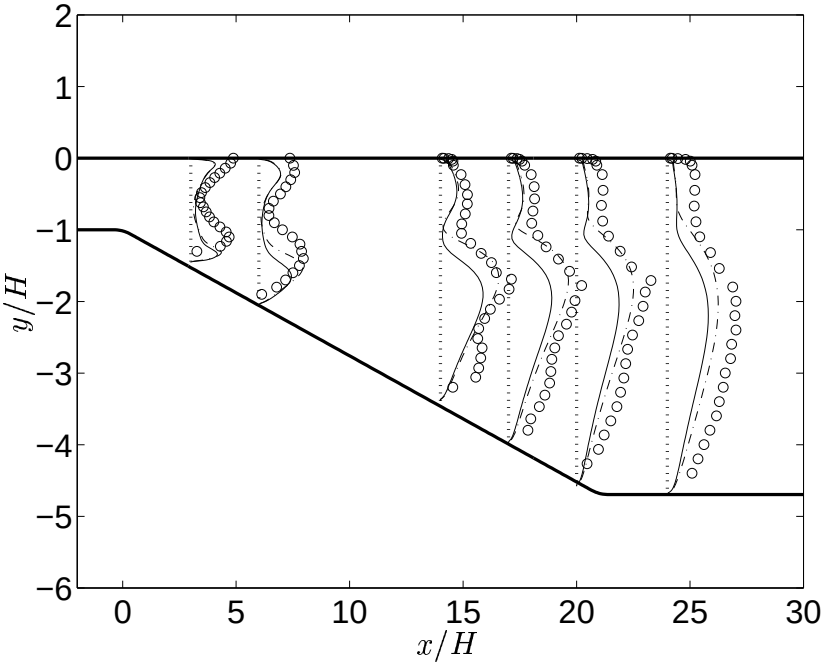

(a) Reynolds stress $\overline{uu}$

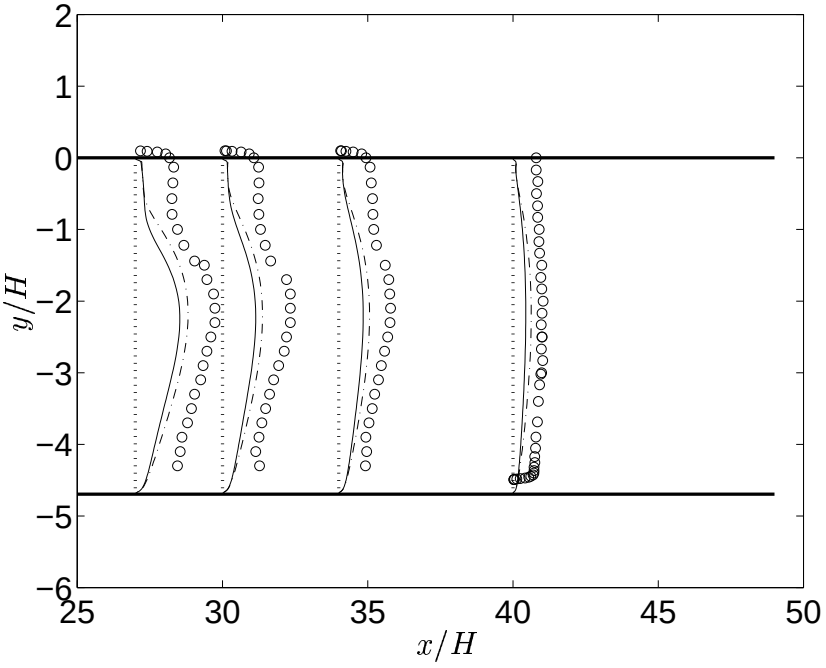

(b) Reynolds stress $\overline{uu}$

Figure 5.14: Reynolds stress $\overline{uu}$. Solid line: $k-\omega-\overline{v^2}-f$; dashed line: modified $k-\omega-\overline{v^2}-f$; ∘: experimental data [2].

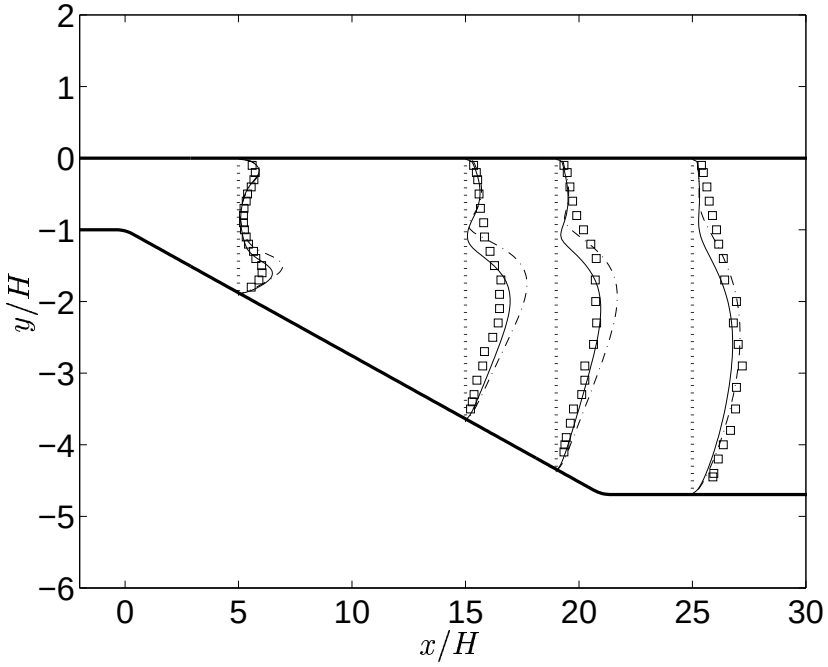

(a) Reynolds stress $\overline{vv}$

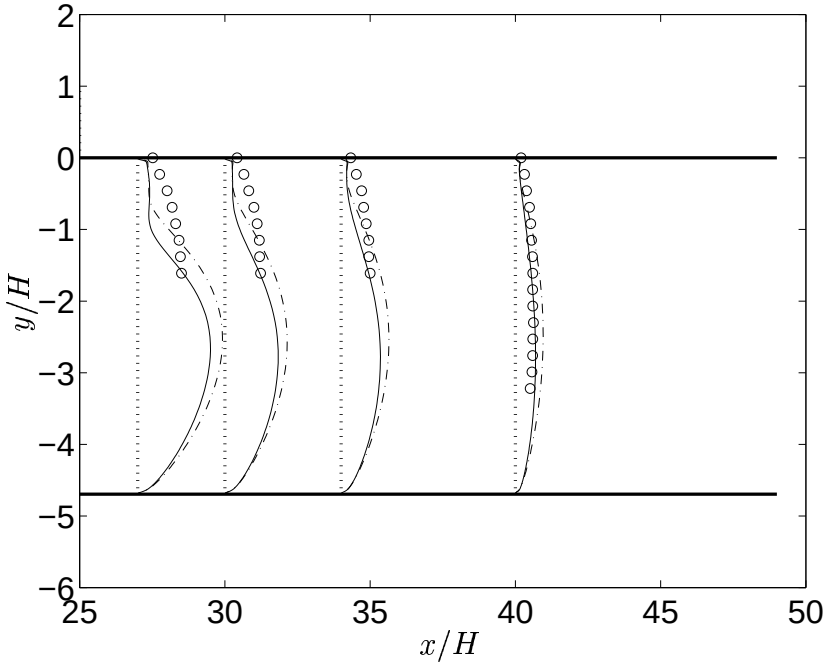

(b) Reynolds stress $\overline{vv}$

Figure 5.15: Reynolds stress $\overline{vv}$. Solid line: $k-\omega-\overline{v^2}-f$; dashed line: modified $k-\omega-\overline{v^2}-f$; ∘: experimental data [2]; □: experimental data [22].

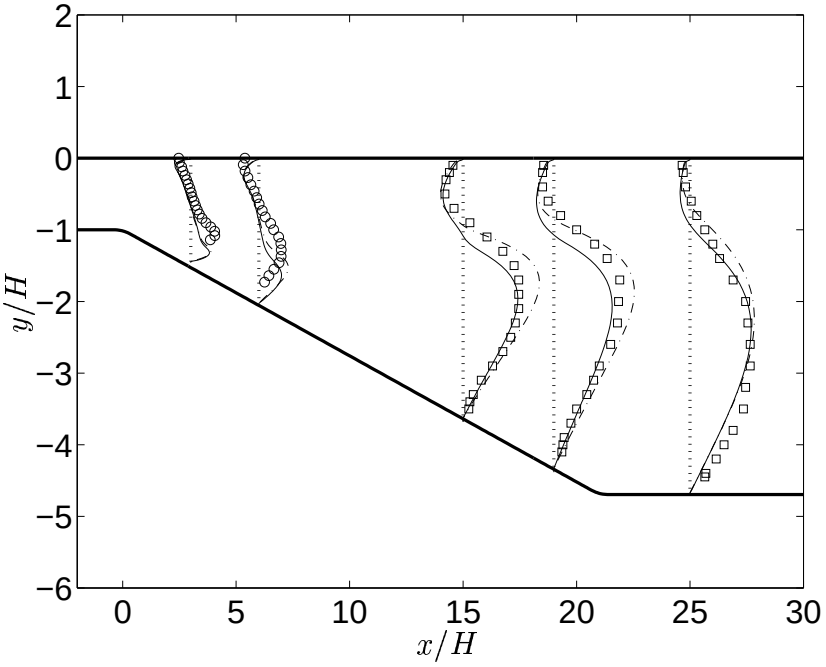

(a) Reynolds shear stress $\overline{uv}$

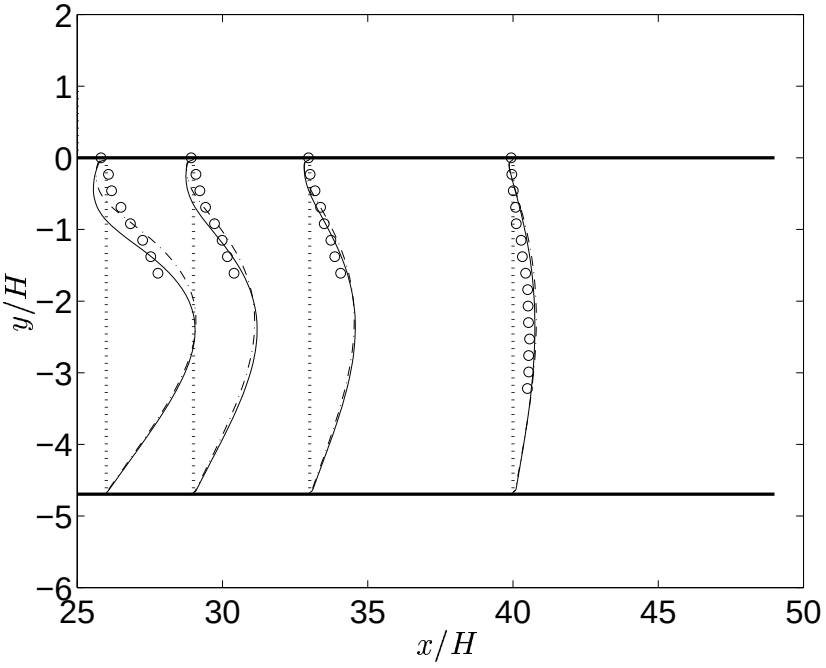

(b) Reynolds shear stress $\overline{uv}$

Figure 5.16: Reynolds shear stress $\overline{uv}$. Solid line: $k-\omega-\overline{v^2}-f$; dashed line: modified $k-\omega-\overline{v^2}-f$; ∘: experimental data [2]; □: experimental data [22].

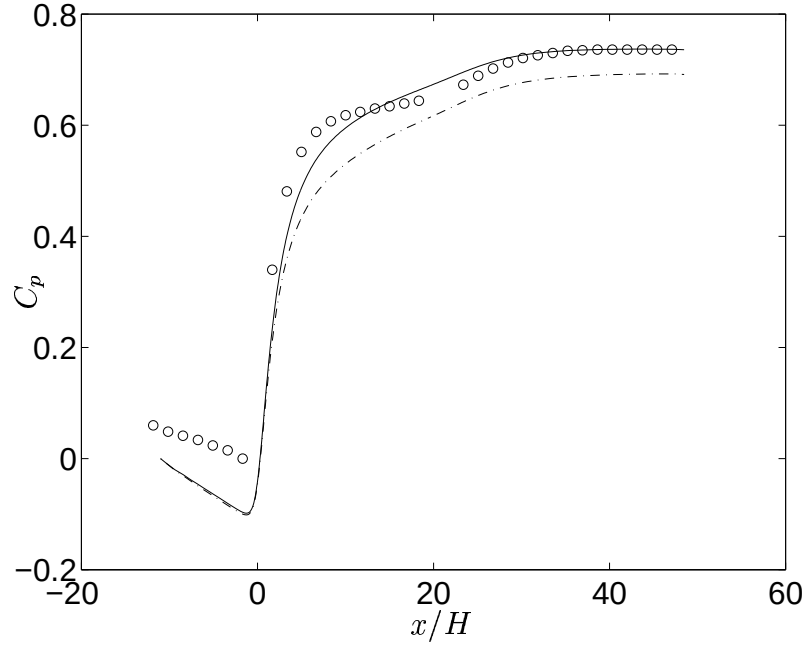

(a) The pressure coefficient C_p

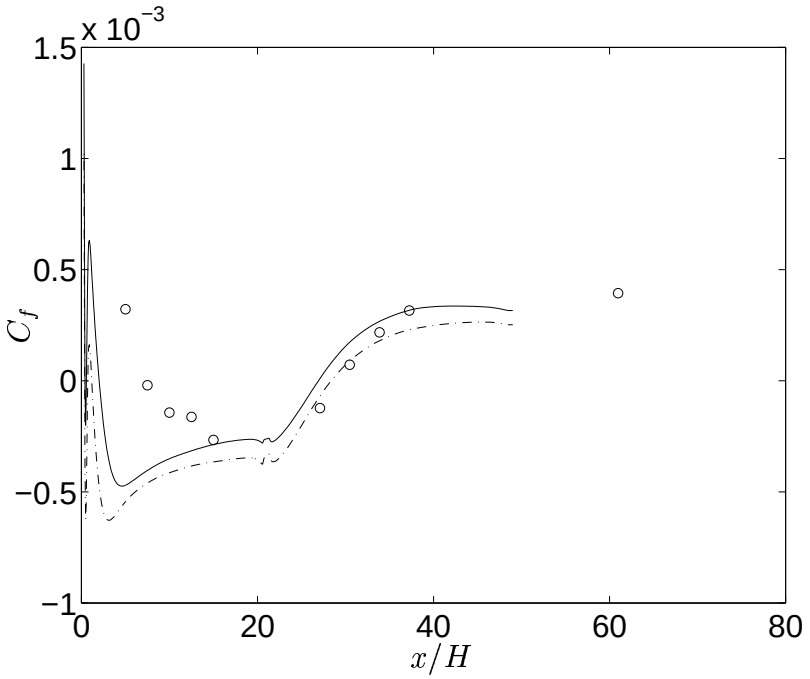

(b) The skin friction coefficient C_f

Figure 5.17: pressure coefficient and skin-friction. Solid line: $k-\omega-\overline{v^2}-f$; dashed line: modified $k-\omega-\overline{v^2}-f$; $\circ$: experimental data [2].

Chapter 6

Conclusions

In the present work, a new $k-\omega-\overline{v^2}-f$ model which has more appealing boundary condition of ω had been developed. The model constants were determined by tuning the results to match the DNS data of fully developed channel flow. The results of a fully developed channel flow suggest that the model is more viscous as it under-predicts the Reynolds shear stress in the near-wall region.

The mesh dependence study revealed the sensitivity of the model to the inlet boundary condition and the wall boundary condition of ω.

As the model is intended for computing complex engineering flows, the performance of the model has been assessed by computing a separated flow in an asymmetric plane diffuser. The results are shown to be in good agreement with the experimental data. The model was able to capture the separation from the inclined wall. The separation point was detected too early in comparison with experimental data. This suggests that a modification is needed to predict the proper behavior of Reynolds stresses.

Bibliography

[1] A. SVENINGSSON. *Analysis of the Performance of Different $\overline{v^2} - f$ Turbulence Models in a Stator Vane Passage Flow,* Licentiate thesis, Department of Thermo and Fluid Dynamics, Chalmers University of Technology, Sweden, 2003.

[2] C. U. BUICE AND J. K. EATON. *Experimental investigation of flow through an asymmetric plane diffuser,* TSD-107,Dept. of Mech. Engineering,Stanford University, USA, 1997.

[3] D. A. ANDERSON, J. C. TANNEHILL AND R. H. PLETCHER. *Computational Fluid Mechanics and Heat Transfer,* Hemisphere Publishing Corporation, USA, 1984.

[4] D. C. WILCOX. *Turbulence Modeling for CFD, 2nd ed.* DCW Industries Inc., USA, 2002.

[5] D. C. WILCOX. *Reassessment of the Scale-Determining Equation,* AIAA Journal, 26:1299-1310, 1988.

[6] D. D. APSLEY AND M. A. LESCHZINER. *Advanced Turbulence Modelling of Separated Flow in a Diffuser,* Flow, Turbulence and Combustion, 63: 81-112, 1999.

[7] D. R. LAURENCE, J. C. URIBE AND S. V. UTYUZHNIKOV. *A robust Formulation of the $\overline{v^2} - f$ Model,* private communication.

[8] F. S. LIEN AND G. KALITZIN. *Computation of Transonic Flow with the $\overline{v^2} - f$ Model,* International Journal of Heat and Fluid Flow, 22, 53-61, 2001.

[9] G. KALITZIN. *Application of the $\overline{v^2} - f$ Model to Aerospace Configurations,* Center for Turbulence Research Annual Research Briefs, 1999.

[10] G. LACCARINO. *Predictions of a Turbulent Separated Flow Using Commercial CFD Codes,* Journal of Fluid Engineering,Vol.123,819-828, 2001.

[11] H. NILSON. *A numerical Investigation of the Turbulent Flow in A Kaplan Water Turbine Runner,* Licentiate thesis, Department of Thermo and Fluid Dynamics, Chalmers University of Technology, Sweden, 1999.

[12] H. J. KALTENBRACH, M. FATICA, R. MITTAL, T. S. LUND AND P. MOIN. *Study of Flow in A Planar Asymmetric Diffuser Using Large Eddy Simulation,* Journal of Fluid Mechanics, Vol. 390, 151-185, 1999.

[13] H. K. VERSTEEG AND W. MALALASEKERA. *An introduction to Computational Fluid Dynamics - The Finite Volume Method,* Longman Scientific & Technical, Harlow, England, 1988.

[14] W. P. JONES AND B. E. LAUNDER. *The Prediction of Laminarization with a Two-Equation Model of Turbulence ,* International Journal of Heat and Mass Transfer, Vol. 15, 301-314, 1972.

[15] J. C. U. TORRES. *An Industrial Approach to Turbulence Modelling for Unstructured Finite Volumes Methods for CFD,* Internal Report, Dpet. of Mech. Aerospace and Manufacturing Engineering, UMIST.

[16] L. DAVIDSON. *An Introduction to Turbulence Models,* Technical Report, Dept. of Thermo and Fluid Dynamics, Chalmers University of Technology, Sweden, 2003a.

[17] L. DAVIDSON. *Computational Fluid Dynamics of turbulent Flow,* Lecture notes, Dept. of Thermo and Fluid Dynamics, Chalmers University of Technology, Sweden, 2003b.

[18] L. DAVIDSON AND B. FARHANIEH. *CALC-BFC: A Finite Volume Code Employing Collocated Variable Arrangement and Cartesian Velocity Components for Computation of Fluid Flow and Heat Transfer in Complex three-Dimensional Geometries,* Report 95/11, Dept. of Thermo and Fluid Dynamics, Chalmers University of Technology, Sweden, 1995.

[19] L. DAVIDSON, P. V. NIELSN AND A. SVENINGSSON. *Modification of the $\overline{v^2}-f$ Model for Computing the Flow in A 3D Wall Jet,* Turbulence, Heat and Mass Transfer 4, 577-584, 2003.

[20] M. FATICA, H. J. KALTENBACH AND R. MITTAL. *Validation of Large Eddy Simulation in A Plane Asymmetric Diffuser,* Annual Research Briefs, Center for Turbulence Research, Stanford, 1997.

[21] N. MANSOUR, J. KIM AND P. MOIN. *Reynolds Stress and Dissipation Rate Budgets in A Turbulent Channel Flow,* Journal of Fluid Mechanics 194, 15-44, 1988.

[22] S. OBI, H. OHIMUZI, K. AOKI AND MASUDA. *Turbulent Separation Control in A Plane Asymmetric Diffuser by Periodic Perturbation,* Engineering turbulence Modelling and Experiments, Elsevier, 1993a.

[23] P. A. DURBIN. *Near-Wall Turbulence Closure Modeling Without Damping Functions,* Theoretical and Computational Fluid Dynamics 3, 1-13, 1991.

[24] P. A. DURBIN. *Separated Flow Computations with the* $k - \varepsilon - \overline{v^2}$ *Model,* AIAA Journal, Vol. 33, 659-664, 1995.

[25] R. D. MOSER, J. D. KIM AND N.N MANSOUR. *Direct Numerical Simulation of Turbulent Channel Flow up to* $Re_\tau = 590$*,* Physics of Fluids A, 11:943-945, 1999.

[26] S. T. JAYARAJU. *Formulation and Implementation of A* $\overline{v\theta} - g$ *Model to Improve the Wall Normal Turbulent Heat Flux Predictions in A Fully Developed Channel Flow,* M.Sc. Thesis, Department of Thermo and Fluid Dynamics, Chalmers University of Technology, Sweden, 2003.

[27] J. P. VAN DOORMAL AND G. D. RAITHBY. *Enhancements of the SIMPLE Method for Predicting Incompressible Fluid Flows,* Numerical Heat Transfer, 7:147-163, 1984.